DESIGN AND CHARACTERISATION OF A SMART SUN-TRACKING SYSTEM FOR MOBILE PLATFORMS

By

HO MING CHENG

A dissertation submitted to the Department of Electrical & Electronics Engineering,
Lee Kong Chian Faculty of Engineering & Science,
Universiti Tunku Abdul Rahman,
in partial fulfillment of the requirements for the degree of
Master of Engineering Science
August 2017

ABSTRACT

DESIGN AND CHARACTERISATION OF A SMART SUN-TRACKING SYSTEM FOR MOBILE PLATFORMS

Ho Ming Cheng

This dissertation investigates the feasibility of adopting a new concentrated photovoltaic (CPV) design to harness solar energy efficiently on mobile platforms. As compared to the non-mobile platform, solar tracking on a mobile platform is much more challenging but rewarding. The major design issue is to track the sun under the conditions of continuously changing in the coordinate and direction of the mobile platform so that the CPV system can extract the maximum amount of solar irradiation from time to time. To detect such changes of coordinate and direction, digital compass and GPS sensor are employed in the system to update the orientation of mobile platform where the CPV system are located and it enable the sun tracking activity to maintain the good tracking accuracy. These sensors are subject to the different kinds of interferences from the surroundings as well as road conditions which lead to various noises to the signal data even though a high precision sensor is used, and hence a filtering mechanism is developed to smoothen the data. In the case of mobile platform, we show that it is essential to incorporate a timing control scheme for dynamic sun tracking system to ensure effectiveness and efficiency. The result shows that the prototype of our design can to achieve a pointing error of 8.086 mrad in stationary state and 72 mrad in mobile state.

ACKNOWLEDGMENTS

I would like to thank my supervisor Dr. Lai An Chow, for his excellent guidance, caring, patience, and providing me with an excellent atmosphere for doing research. I would also like to thank my co-supervisor, Prof. Dr. Chong Kok Keong, who let me experience and explore more in the field of the renewable energy.

I would also like to thank Dr. Wong Chee Woon, Dr. Yew Tiong Keat for the guidance in the field of renewable energy and also the help on the installation of the hardware in this project.

I would also like to thank my coursemates and friends who help out during the design of the project, the experiments and the data collection for this project. Without all of them, it would be hard for me to complete all alone.

Finally, I must express my very profound gratitude to my mom and to my boyfriend for providing me with unfailing support and continuous encouragement throughout my years of study and the process of researching and writing this dissertation. This accomplishment would not have been possible without them. Thank you.

DECLARATION

I hereby declare that the dissertation is based on my original work except for quotations and citations which have been duly acknowledged. I also declare that it has not been previously or concurrently submitted for any other degree at UTAR or other institutions.

Name _____

Date _____

APPROVAL SHEET

This dissertation entitled "**DESIGN AND CHARACTERISATION OF A SMART SUN-TRACKING SYSTEM FOR MOBILE PLATFORMS"** was prepared by HO MING CHENG and submitted as partial fulfillment of the requirements for the degree of Master of Engineering Science at Universiti Tunku Abdul Rahman.

Approved by:

_____
(Dr. Lai An Chow)
Date:……..
Supervisor
Department of Electrical & Electronics Engineering
Lee Kong Chian Faculty of Engineering & Science
Universiti Tunku Abdul Rahman

_____
(Prof. Dr. Chong Kok Keong)
Date:……..
Co-supervisor
Department of Electrical & Electronics Engineering
Lee Kong Chian Faculty of Engineering & Science
Universiti Tunku Abdul Rahman

LIST OF EQUATION

LIST OF TABLE

LIST OF FIGURES

TABLE OF CONTENTS

CHAPTER ONE

INTRODUCTION

1.0 Introduction

Dependency on fossil fuels is always the major concern in many globalized meetings on the global warming and environment pollution issues. This global warming issue has been a priority concern to the community and immediate solution on this issue is a necessity. Global warming is caused by carbon emissions and one of the major outputs of carbon dioxide is from burning of fossil fuels. Fossil fuel is used to produce the electricity as well as to provide the source of energy for us to commute around every day. On the other hand, fossil fuels have caused serious environmental pollution, contaminating not only human being but also any living creatures. The pollutants of environmental pollution come in gaseous, solid and liquid forms; it can be categorized into oil pollution, air pollution, water pollution as well as soil pollution. As the major source of pollutants, fossil fuel can be replaced with renewable energy as from time to time the cost of manufacturing of renewable energy plantations or stations is getting lower while the efficiency of the system increases. In the year of 2015, investment in clean energy broke new records and is now twice as much global funding as fossil fuels. More and more researches are focusing on the renewable energy as non-renewable

energy is getting lesser and lesser while renewable energy is everywhere. Natural resource is the main source of renewable energy. Generally, clean technology covers a broad range of technologies which can be classified into four major divisions; i.e. renewable energy generation and energy storage, energy efficiency, carbon capturing and recycling. In our studies, we will be focusing on the using renewable energy to generate electricity on mobile platforms.

Generating electricity from the renewable energy could be hard and often restrained by the nature. Power generation by renewable resource is to transform the collected natural resources to electricity. There are multiple ways of power generations, such as hydroelectric, wind, geothermal, solar, biomass and waste. These ways are now in use world widely based on the terrain and the natural condition of the selected area. From the latest REN21 report (Adib, et al., 2016), the total global output of power and global capacity has been increasing world widely and this renewable energy power generation is now providing a significant share of electricity in many countries, including developing countries like China and Brazil. Undeveloped terrains are used to build the renewable energy power stations to provide the electricity to main cities in the countries. Among the multiple ways of power generation, we focus on the solar energy generation in this study.

For the category of power generation, there are still a lots of countries are depending on the fossil fuels. Generating electricity would be the major usage of fossil fuels; power for transportation would be the second in the

power generation by using solar energy, there are two main types of solar tracker, non-mobile solar tracking system as well as mobile solar tracking system. There are multiple designs of non-mobile solar tracking system, such as solar power tower, parabolic trough, large dense array and large concentrated solar system. These designs usually are huge in size and take up lots of spaces so these non-mobile solar trackers are usually installed in rural areas. To fully utilize the natural resources, mobile solar trackers have come into action. Mobile solar tracker is an on-the-go solar tracking system that ultimately to generate electricity wherever it is located. Design of the mobile solar tracker is usually smaller in size as compared to non-mobile solar tracking system, to promote the mobility as well as the advantage of generating electricity anytime and anywhere provided with sun irradiation. Furthermore, this mobile solar tracking system can be installed on the mobile platforms and generate electricity as the source of power for vehicles whether is during static or travelling.

There are few reasons why mobile solar tracking system is likely to have more advantages over the non-mobile solar tracking system. For non-mobile solar tracking system, as they are huge in size, they are always limited to certain area with open space, while for mobile solar tracking system, the size is contrarily much smaller and it is portable and not restrained to remote areas or terrains only. Moreover, non-mobile system usually incurs much higher manufacturing and installation costs while mobile solar tracking system has a low entry barrier, also maximizing the potential of collected sun irradiation as much as possible with the portable size. The mobile solar energy

system is flexible and able to generate electricity anytime and anywhere while the non-mobile solar energy system cannot. For non-mobile solar tracking system, it could not maximize the usage of the natural resources as it is restricted to certain area and there is some hidden cost, including the maintenance, cost of land, wiring and storage of the power generated; in contrast, mobile solar tracking system is portable and it can be installed on mobile platforms, such as trucks and ships, using the generate electricity to reduce the transportation cost. Furthermore, but not limited to, mobile solar energy system could potentially reduce transportation cost by a significant percentage through different creative uses of it as there is more and more hybrid or electric vehicles (EVs) on the road currently. There are lots of mobile solar transportation ideas available and many big companies are on their way of transforming the ideas into a real product. Without a tracking scheme, the solar system always has a cosine loss also it might be shaded as it only facing at on static direction. Mobile solar tracking system is able to resolve this issue and maximizing the collection of sunlight to face the sun at the right direction.

1.1 Problem Statement

There are a few challenges to design an effective mobile solar tracking system. Identifying the orientation and alignments are very important for the solar tracking system so that the system can always point to the Sun and the key to success is the ability to find the real north when the system is moving.

From the non-mobile solar tracking system designs, we know that geographical information is an essential need in the calculation of the rotational angles of sun trajectory. Detection of the geographical location is important to get the correct rotational angles. Secondly, unlike the non-mobile solar tracking system settings, the mobile solar tracking system is less likely to be at the exact correct alignments. One of the important alignments is the real north orientation, so it is critical for mobile solar tracking system to detect the direction with respect to the north from time to time. Also, as the mobile solar tracking system is catered for mobile platforms, the real north detection is no longer a constant, but a function with respect to time. Road condition is never perfect but bumpy in practice and abrupt changes, roundabout and multiple turnings on a short path are unavoidable. These road conditions are essential to be included in the design of mobile solar tracking system algorithm or mechanisms as they are very common.

1.2 Research Objectives

There are three objectives that we intend to achieve in this study.

- To design the software and hardware of the mobile solar tracking system.

The design of the mobile solar tracking system includes both the hardware the software. For the software of the mobile solar tracking system, we have sensor readings, filtering algorithm, computation of the rotational angles of sun trajectory, choice of the control system and also the control

system for the solar energy receiver and the hardware controlling system. While for the hardware, we need to design a solar energy receiver that can effectively collect the sun radiation to the solar cells for electricity generation.

- To analyze the tracking performance of the mobile solar tracking system.

Performance of the software and hardware of the mobile solar tracking system has to be verified. With the implementation of the solar energy receiver, we not only collected the current or voltage readings to analyze the performance of the algorithm applied on the mobile solar tracking system, but also captured solar images to analyze the error of tracking of the mobile solar tracking system based on different set of variable or experiment designs.

- To evaluate the performance of mobile solar tracking system.

From the analysis collected in the second objective, we can evaluate the performance of each experiment designs and choose one best setup to conclude the usability and effectiveness of the mobile solar tracking system. Furthermore, we are able to evaluate the condition of the system as well as the environment condition based on the captured and analyzed results.

CHAPTER TWO

LITERATURE REVIEW

2.0 Literature Review

2.1 Solar System in the World

There are various types of solar energy systems available in the industry as well as the commercial market. Depending on the needs, the solar energy system can provide thermal energy as well as the electricity. One of the common examples is the solar panel that installed on the roof top of residential housing area. On the other hand, some of the large scale solar energy systems like large solar energy mining in Ukraine, large-scale solar heating and energy storage system in Mexico, Ivanpah Solar Electric Generating System and so on.

2.1.1 Photovoltaic

Solar cell and solar panel are something no longer uncommon as it has been introduced and applied for a few decades. Photovoltaic (PV) is best known as a method for generating electric power by using solar cells to convert energy from the sun into a flow of electrons. As the light or photons striking on certain compound or particular metals, it causes the surface of the material to emit electrons while it striking on the other compounds that accepting electrons. It is the combination of these two compounds that can be

made use of to cause electrons to flow through a conductor and thereby creating electricity. The phenomenon is called the photo-electric effect, and photovoltaic means sunlight converted into a flow of electrons or electricity. Efficiency of photovoltaic system has slowly increased from time to time as the needs from industrial to commercial and residential are increasing.

Figure 2.1 Solar Panel

Solar panel is built from an array of solar cells. For each of the solar panel, it can produce DC voltage of typically 25 to 40 volts and with a rated output of between 150 and 250 W_p. To supply electricity into the mains electricity system, the DC output from the solar panel has to convert to AC at the correct voltage and frequency. An inverter will be added to do the conversion.

The use of solar panel increases as it is relatively easy to install and requires very low maintenance. For each of the solar panel modules are

reliable and have a long life span; also solar panels can generate electricity without introducing waste or pollution. One of the useful characteristic of solar photovoltaic power generation is that it can be installed on any scale as opposed to conventional forms of power generation that require large scale plant and maintenance. One of the reason why the grid connected PV system is mounted on the roof or walls of building is to minimize the shading of the PV system without using land that could be used for other purposes.

Conventional solar panel is considered as low-cost silicon PV. In the high concentrating PV (HCPV), it is claimed to be lower the cost but increases the efficiency (Leone, 2011). It reduces the active area needed form the photovoltaic element, low demand in the usage of raw material (manufacturing of the solar cell), able to work well in conjunction with solar tracking system as well as having best efficiency ratio compared to the low-cost silicon PV. With this high efficiency solar cell, the design of the solar tracking system is reduce in size also increase the accuracy to increase the overall performance. The high concentration PV cell needs an active cooling system to remain the effectiveness and efficiency as the concentrated sunlight is pointing directly onto the PV cell and it need to avoid overheating. For design using the high concentrating PV, it is required to have a cooling system design included to avoid thermal destruction of PV cell. For installation area around the equator or hot environments, HCPV is more efficient than normal PV cells.

In Rodrigoa et al's design, before the HCPV module, there are two concentrating optics are used, Fresnel lens and secondary prism (P.Rodrigoa, et al., 2013). In Rumyantsev et al's research, they are using Fresnel lens as primary optical element and a plane convex lens as the secondary optics (V.D.Rumyantsev, et al., 2010). The 2.3mm diameter cell is able to achieve 23.4% efficiency with the 8-lens module (60mm×60mm Fresnel lens) and a 8mm focal length secondary optics. In Schultz et al's design, Fresnel lens is the primary optics and a refractive optic as secondary optics (Schultz, et al., 2012). The HCPV cell used in this design achieve cell and module efficiency of 38.4% and 24.2% respectively.

2.1.2 Examples of Large Scale Solar PV System

Activ Solar's 100 MW Perovo PV plants (Roselund, 2013) in Ukraine taking up to 200 hectares of lane and it is one of the largest single-site PV plant in Europe. This system uses 440,000 crystalline solar PV modules and it can produce up to 132,500 Megawatt-hours of clean and renewable electrical energy per year. This system also helps avoiding up to 105,000 tons of carbon emissions.

Figure 2.2 Activ Solar's Perovo PV plant (Roselund, 2013)

Arcon-Sunmark, Denmark's large-scale solar heating specialist recently completed a 5.1MW (peak) solar heating plant at the Penoles' La Parrena copper mine in Mexico (Golubova, 2016). This plant has a collector field of 6.27 m2 with a total of 456 collectors and it is equipped with a 660 m3 of storage tank for storing surplus heat.

Figure 2.3 Penoles' La Parrena Solar Heating Plant (Golubova, 2016)

Spain's Arnedo Solar Plant (Lewis, 2016) can produces an impressive of 34GWh every year, which it power 12,000 households and prevent 375,000 tones of CO_2. This facility uses land of 70 hectares and completed with

172,000 panels.

Figure 2.4 Arnedo Solar Plant in Spain (Lewis, 2016)

Moura photovoltaic power station in Portugal using 190,000 panels on fixed structures and 52,000 on a single axis trackers. It occupies an area of 130 hectares producing 88 GWh of electricity energy per year.

Figure 2.5 Moura photovoltaic power station, Portugal

One of the developing countries, India, announced that by 2017 a 648 MW solar power plant will be done which covers an area of 10 km^2 at Kamuthi (Thompson, 2016), Tamil Nadu. It is estimated to produce enough electricity to power about 150,000 homes.

The disadvantage of large scale solar PV system is that the land area required is really big and this system is usually located at rural area to avoid residential area. For each of the solar PV, the cleanliness needs to be maintained to keep the efficiency of each of the solar PV. As a result, the use of water becomes unavoidable and a big challenge for some of the solar power plant as the choice of land of the solar power plant is mostly deserted away from the source of water. In addition, solar PV has a life time up to 30 years; the disposal of the material is yet to be a concern to the industry. It is claimed by the manufacturers that the high value materials are recycled. However, if it is not handled and disposed properly; the materials could pose serious environmental or public health threats.

2.1.3 Solar Tracking System

Solar energy harvesting can be as simple as just placing a solar panel on the roof top, or complicated and large system like a large solar plant. In simple conventional design, solar energy receiver is often to be fixed mount on certain position and from the movement of the Earth, this fixed mount solar energy receiver always have a cosine angle of losses as there is more chance of the solar panel is on the less-than-optimal angle (Bushong, 2016).

Tracking system is able to compensate the loss from the fixed mount solar energy receiver. Tracking system minimizes the angle of incidence, angle between the incoming sunlight and panel, increasing the amount of energy to be produced (Zipp, 2013). Tracking system is able to generate more electricity than the fixed mount solar panel as it increases its exposure to direct sun irradiance. In Ingole's research, tracking system is able to generate 40% more electricity than the fixed mount solar panel (Ingole, 2016).

There are two types of trackers, single axis tracker and dual axis tracker (Fedkin, 2016). For single axis tracker, only one axis is adjustable and it is depending on the location that the tracker installed, either horizontal or vertical axis. For dual axis tracker, both horizontal and vertical axes are adjustable to point towards the Sun; it can track the Sun at any location. For high concentrating solar system or large concentrated solar power, these systems need high accuracy to collect the sun irradiance with maximum efficiency.

2.1.4 Concentrated Photovoltaic System

Adding an optical light collector such as lenses or mirrors is able to increase the output of the photovoltaic system whereby it supplies the concentrated light onto the PV cells. The PV cell chosen is HCPV cell to maximize the electricity harvesting. Two known optical instruments set up are Fresnel lens and Cassegrain reflector.

2.1.4.1 Fresnel Lens

One of the optical instruments used to focusing the sunlight is Fresnel lens. It can help in the concentration of sun irradiation. Fresnel lens consists of a series of concentric grooves etched into plastic. It can be in small as well as large sizes and it is light weighted. Fresnel lens replaces the curved surface of a conventional optical lens with a series of concentric grooves. The contours are acting as individual refracting surfaces and bending the parallel light rays to a common focal length. The weight and thickness are reduced as compare to a standard focusing lens.

Fresnel lens is widely used in the CPV (Concentrated Photovoltaic) System. Fresnel lens is designed to improve the concentration of sun light coming from many different angles onto a single point or line. In CPV system, Fresnel lens is often use to concentrate the sunlight and making sure the concentrated point fall onto the solar cell to generate more electricity from the solar power as it increases the amount of sunlight striking on the solar cell.

The use of Fresnel lens onto the CPV system created three competitive advantages. First, with the use of Fresnel lens in concentrating the sunlight before falling onto the solar cell, it requires less photovoltaic material to capture the same sunlight as the non-concentrating system. Secondly, it makes the use of high efficiency but expensive multi-junction cells economically viable due to smaller space requirements. Lastly, the cost for the overall CPV system will be much lower as the optics is less expensive than the solar cell.

Huang et al's paper discussed on design analysis on Fresnel lens concentrates sunlight and strikes on a strip of PV cell (Huang, et al., 2011). They predicted the sun irradiance distribution and current flow distribution on PV cell, checking on how is the distribution of sun irradiance may affect the concentration ratio. A biaxial-type concentrated solar tracking system is designed by Cheng et al. using the Fresnel lens to concentrate sunlight heating up the Stirling engine (Cheng, et al., 2016). In Sanchez Vega's design, Fresnel lens is used to concentrate the sunlight for a small scale solar concentrator (Sanchez Vega, 2016). The design uses a spot type Fresnel lens and with heat absorber instead of PV cells, concentrating the sunlight to use as solar thermal energy.

2.1.4.2 Cassegrain Reflector

Another type of optical instruments can be used in focusing the sunlight is Cassegrain reflector. Cassegrain reflector is consists of a concave mirror as primary optics and a convex mirror as secondary optics. This design is often use in the design of telescope but it can also provides highly concentrated sunlight to the high concentrated PV cell in the design of solar tracking system. The first mirror is working as the collector to collect the sunlight while second mirror is working at as concentrator, concentrate the collected sunlight onto the solar cell or any other PV equipment.

In Roman et al's design, a short focal length primary parabolic collector is used while hyperbolic reflective element is used as the secondary optic to redirect the sun irradiance (Roman, et al., 1995). In the ray tracing

analysis, 70 to 75% of the collected sunlight from the primary optic is able to focus within a 0.5m radius. The design of Cassegrain has its disadvantage, so in Shanks et al's design; a solid transparent homogenizer is added to give tracking tolerance towards the two stage reflector design (Shanks, et al., 2015). In the simulation, for ±1° of tracking error, the optical accuracy able to achieve 84.82 – 81.89% while with ±1.5° tracking error the optical accuracy is 55.49%. For Zhang et al's design, a double pyramid is added before the PV receiver to eliminate the dark image caused by the secondary optic (Zhang, et al., 2016). The block ratio is 20% when the primary mirror length is 89m and getting a concentration ration of 118.96 in the simulation.

2.1.5 Concentrated Solar Power

Concentrating solar power plants use mirrors to concentrate the energy from the sun and drive the traditional steam turbines or engines to create electricity. The solar power plants generate electric power by using mirrors to concentrate the solar energy and convert it into high-temperature heat. The heat will then be channeled through a conventional generator. The collection of the heat can be stored and used to produce electricity when it is needed.

Parabolic trough is a concentrating solar power system that was used widely since 1980's. Parabolic trough consists of few parts, parabolic reflectors or mirrors, receiver tube and tracking system (Wang, 2008). The parabolic reflectors or the U-curved mirrors are the main component as it focuses the rays of sun into the absorber pipe. There is fluid in the receiver tube, normally is synthetic oil, it is circulating inside and it is heathen up by

the sun then pumped through heat exchanger to generate steam which used to produce electricity in conventional turbine. Tracking system is important for parabolic trough power plant as it need to make sure that direct sun irradiance fall on the parabolic reflectors to give the best result of solar energy collection. Parabolic trough solar power plant uses one-axis tracking system while point concentrating system usually applies two-axis solar tracking.

Power tower (Parkinson, 2013) is also known as central receiver, it is equipped with many large and flat heliostats to track the sun and focus the sunlight onto the receiver. The heliostats are made of mirrors that follow the instruction of the tracking system to achieve the best result in generating electricity. On the receiver, the concentrated light then heats up a fluid which is very high in temperature. This hot fluid can be used to make steam for electricity generation immediately or stored for later use as the fluid used can retains heat efficiently. Heliostats applied one axis tracking or two axis tracking based on different system design.

Dish system (Mercer, 2012) is the other type of concentrated solar power system that used mirrored dishes to concentrate the sunlight onto the receiver. The receiver is mounted on the focal point of the dish. In order to capture the maximum amount of solar energy, the dish is usually programmed to tracks the sun across the sky. The receiver then integrated into a high efficiency combustion engine and it has thin tubes containing gases that run along the outside of the engine’s four piston cylinders. When the concentrated sunlight falls on the receiver, it heats up the gas in the tubes to high

temperature, expands and drives the pistons of the cylinders. The pistons turn a crankshaft which is a mechanism to drive the electricity generator.

Figure 2.6 Dish System

In the concentrated solar power plant, cooling system is needed as the temperature of the concentrated collection of sunlight will reach up to $1000°C$, and making sure the effectiveness and efficiency of the whole solar power plant. Cooling system that applied is by using water, but as the location of the plant is usually deserted, to cost of transporting water and cooling the plant is high. Later, dry cooling system which uses air to cool down the system is applied to reduce the use of water in the plant.

2.1.3.1 Mojave Solar Project

Mojave Solar Project (U.S. Department of Energy, 2011) is one of the parabolic trough solar plants. It is located in 100 miles northeast of Los Angeles, California. The size of the solar plant is 1,765 acres. Production of electricity in gross is 280 MW and it can serve up to 91,000 households and eliminating the emission of more than 223,500 tons of carbon dioxide annually.

Figure 2.7 Mojave Solar Project (U.S. Department of Energy, 2011)

Collectors concentrate the sunlight that strike on the parabolic trough onto the receiver tubes which deliver the heat into to central power plant via the heat transfer fluid. The generation of electricity is occurred on the conventional steam turbines after the receiver tubes. For this project, the manufacturer also claims that they used 80% less water than other available design.

Figure 2.8 Parabolic Trough in MOJAVE

2.1.3.2 Ivanpah Solar Electric Generating System

Ivanpah Solar Energy Generating System (BrightSource Limitless, 2014) is the largest example of solar thermal power generation in the world currently. Ivanpah Solar Energy Generating System is located at Ivanpah Dry Lake, California, United States; the size of the whole system is approximately 3,500 acres or equal to 14.2 km^2. Power production of this large solar system is 377 MW (net) and it can serve up to 140,000 homes annually. This system nearly doubles the amount of commercial solar thermal energy generated in United States.

Figure 2.9 Ivanpah Solar Tower

This solar energy generating system produces electricity by creating high temperature steam to turn a conventional turbine. There is 300,000 pieces of software controlled mirrors tracking the sun in two dimensions and reflecting the sunlight to the boilers that sit atop three 459 foot tall towers. When the concentrated sunlight strikes at the boilers' pipes, it will heat the water can creating superheated steam. Then, the high temperature steam is piped from the boiler to a standard turbine where the electricity is generated. The generated electricity will be carried to homes and businesses via the transmission lines.

Ivanpah Solar Energy Generating System optimized the solar field design by adding the taller towers and it uses less land than their competing solar technologies, including photovoltaic and parabolic trough. It improves

the air quality by avoiding millions of metric tons of carbon emissions over the solar plant's life. This solar plant will have reduced air pollutants, such as nitrogen oxides (NO_x) and sulphur oxides (SO_x) than a natural gas-fired power plant. It employs a dry-cooling process, so it uses up to 95% less water as compared to other competing wet cooled solar thermal plant. It uses air instead of water to condense steam and the steam production cycle is a closed-loop system, with all the water recycled back into the system, while general conservation measures help to further reduce water usage. Furthermore, this project has the limited impact on the site whereby it retains the majority of the project site's natural landscape than extensive grading and concrete foundations. This allows the land to retain its natural land contours and features.

2.2 Closed Loop, Open Loop and Hybrid System

It is critical to have a sun tracking system to maximize the extraction of solar energy, especially in a high concentrating photovoltaic system whose output is sensitive to the accuracy of the sun tracking system. There are various types of non-mobile strategies have been introduced over the past two decades. The tracking accuracy of the solar tracking system is based on the specification and restriction of the designs. Sun tracking system can be categorized into three big categories; closed-loop, open loop and hybrid solar tracking system. These solar tracking systems usually employ sensors to work as a feedback to control the system, to achieve high tracking accuracy.

Closed-loop system uses a closed loop sensor to work as the feedback to the control system. Sensors like CCD (charge-coupled device) camera, light dependent resistor (LDR) or photo-detector are the closed loop sun tracking systems that capture the solar image or intensity of light to keep track of the Sun's position and send signals to the control system. If the sensors detected that the Sun's position is moving away from the solar energy receiver, it will trigger the system to move to the right Sun's position. An automatic sun tracking system is integrated by Akhmedyarov et al. (Akhmedyarov, et al., 1986) to a solar photoelectric station in Kazakhstan which increases the output power from 357 Watt to 500 Watt. Another example, heliostats designed based on closed-loop scheme with four CCD cameras attached on the target by Kribus et al (Kribus, et al., 2004). This design improved the pointing error of the solar image to 0.1 mrad but it is rather complicated as well as expensive as the solar images needed to be analyzed by the computer in order to generate the correction feedback if the solar image is away. For the analysis, it consumes a lot of computing time and power of computer or control system. On the other hand, Luque-Heredia et al. introduced a sun-tracking error monitoring which uses monolithic optoelectronic sensor for concentration photovoltaic system. This system achieved a tracking accuracy better than 0.1 degree from the case study result but this system is only able to operate on a full clear sky (Luque-Heredia, et al., 2006). Next, a heliostat with an equatorial mount and a closed-loop photo-sensor control system is introduced by Aiuchi et al. From the experimental results, this system estimated to have a 2 mrad tracking error during fine weather, yet this design is not popular as it has the equatorial mount configuration as well as having a complicated

mechanical structure (Aiuchi, et al., 2006). On the other hand, Chen et al. presented studies of digital and analogue sun sensors based on the optical vernier and optical nonlinear compensation measuring principle which have tracking accuracies of 0.02 degree and 0.2 degree for the field view of ±64 degree and ±62 degree respectively (Chen, et al., 2006). The disadvantage in these sensors is that the ranges of degrees are small as compared to the practical sun-tracker which has a dynamic and larger range of degrees. In Ingole's design, she uses Arduino as the main controller and LDRs to detect the light intensity, as a closed-loop sun tracking design (Ingole, 2016). The installation of LDRs is problematic also in the extreme climate conditions, LDRs may easily damage.

From the previous studies, we can see that closed-loop sun-tracking system can produce high tracking accuracy. However, it is possible to lose the feedback signals when the sensor is being blocked or shaded by clouds. To overcome this limitation, open-loop sun trackers are introduced. For open-loop sun tracker, the system calculate the moving path of the sun using special mathematical formula or algorithm involving date, time and geographical information. It does not require any solar image as feedback like the closed-loop sun tracking system. Open-loop sensors are installed to determine the rotational angles of tracking axes as well as making sure the solar collector is positioned at the calculated angles. A two-axis sun tracking system which is introduced by Abdallah et al. uses the open-loop sun tracking scheme (Abdallah & Nijmeh, 2004). In Ingole's design, Arduino is used as the main microcontroller and LDR sensors are used as open-loop sensors (Ingole, 2016).

LDRs generated feedback error voltage for the system to determine which direction has the better light intensity. In the tracking using single axis, the output efficiency increase by 6-7% and tracking by dual axis, the output efficiency increase by 30-40%.

Generally, closed-loop scheme and open-loop scheme have their strengths and weaknesses; this is where hybrid system comes into play. Hybrid systems include both open-loop sensors and closed-loop sensors. In Nuwayhid et al.'s design, it uses computer to calculate the two rotational angles and drive the solar tracker along the polar axis and declination axis which acts as the open-loop scheme while nine light-dependent resistors (LDR) that arranged in circular shape that acts as the closed-loop sensor to make sure the tracker is on the right sun's position (Nuwayhid, et al., 2001). From Luque-Heredia et al.'s design, the system has a mathematical model which uses time and geographical coordinate function to provide feed-forward open-loop estimation of sun's position; it included an error correction routine to secure the high accuracy sun tracking (Luque-Heredia, et al., 2004). Next, Rubio et al came out with solar tracker that has two tracking modes, which is normal tracking mode and search mode. Normal tracking mode has both open-loop scheme and closed-loop scheme to obtain a small sun-tracking error but if the error is larger than the boundary, search mode will be activated. In search mode, the tracker will keep "searching" on the moving axes until it matches the minimum tracking error allowed in the system (Rubio, et al., 2007). Ferdaus et al came out with a design using hybrid dual axis tracking, which one axis is continuously tracking while another only runs once a month

(Ferdaus, et al., 2014). This system is claimed achieves 25.62% more average power gain over the normal static system also 4.2% less power gain compare to continuous solar tracking system.

Furthermore, in Chong et al.'s design (Chong & Wong, 2009), they created a formula for an on-axis solar tracker. The mathematical formula takes date, time as well as geographical information as input parameters. A vanilla implementation of the formula found out that the tracking accuracy is not as good as expected due to a small misalignment occurred during the building of the solar tracker. This is an issue which also occurs in most solar power plants as alignment work of sun-tracking axes is not easy especially on large solar tracker. In order to overcome this problem, they have come out with a general formula to cater for the misalignment from the ideal configurations. This solution made a great improvement as getting precise measurement in manufacturing of the large solar plant is a great challenge that could massively increase the manufacturing cost.

A team of Weber State students, along with Associate Professor McCulley, Julie designed and developed the Mobile Elemental Power Plant (MEPP) where it is a mobile generator that runs on renewable energy (Ogden Publishing Corporation, 2015). The mini-power station is used to replace traditional generators used for camping or as backup power sources. S.Sivasakthi M.E et al. came out with an automatic solar tracking system for power generation using microcontroller and sensor (M.E., et al., 2016). It is equipped with portability whereby it can move to solar illuminated region if

the solar panel is at the shaded region. It uses Atmel microcontroller as the main controller and LDRs to build the system. In B.Suchitha Samuel et al.'s design, PIC microcontrollers are used to control and LDRs to sense the light intensity (Samuel, et al., 2013). It separates the control of the robot system and the tracker, yet the disadvantage of the system is the entire system is monitored and control by PC.

2.3 General Sun Tracking Formula of On-Axis Open Loop Sun Tracking System

This formula is integrated on a dish type hardware prototype, which is the point tracking and using two axes tracking throughout their studies. In this paper, it is claimed that the formula improved the tracking accuracy to 2.99 mrad, which falls below the encoder resolution limit of 4.13 mrad (Chong, et al., 2009).

In the General Sun Tracking Formula, there are a few parameters that are very essential to calculate the right rotational angles. Latitude angle (Φ), hour angle (ω), declination angle (δ) and three orientation angles (φ, λ, ζ) are the variables needed in the calculation. As the hardware prototype used in this study is a dish system which uses two axes solar tracking scheme, it needs to calculate the two rotational angles, Azimuth and Elevation (α, β) angles. Latitude angle can be retrieved from using any available GPS sensor, while the hour angle and declination angle can be retrieved from date and time system.

$$[S'] = [\zeta][\lambda][\phi][\Phi][S] \tag{2.1}$$

$$\begin{bmatrix} sin\alpha \\ cos\alpha sin\beta \\ cos\alpha cos\beta \end{bmatrix} = \begin{bmatrix} cos\zeta & 0 & sin\zeta \\ 0 & 1 & 0 \\ -sin\zeta & 0 & cos\zeta \end{bmatrix} \times \begin{bmatrix} cos\lambda & -sin\lambda & 0 \\ sin\lambda & cos\lambda & 0 \\ 0 & 0 & 1 \end{bmatrix}$$

$$\times \begin{bmatrix} 1 & 0 & 0 \\ 0 & cos\phi & -sin\phi \\ 0 & sin\phi & cos\phi \end{bmatrix} \times$$

$$\begin{bmatrix} cos\Phi & 0 & sin\Phi \\ 0 & 1 & 0 \\ -sin\Phi & 0 & cos\Phi \end{bmatrix} \times \begin{bmatrix} cos\delta cos\omega \\ -cos\delta sin\omega \\ sin\delta \end{bmatrix}$$

$$\begin{bmatrix} sin\alpha \\ cos\alpha sin\beta \\ cos\alpha cos\beta \end{bmatrix}$$

$$= \begin{bmatrix} cos\zeta cos\lambda & -cos\zeta sin\lambda cos\phi + sin\zeta sin\phi & cos\zeta sin\lambda sin\phi + sin\zeta cos\phi \\ sin\lambda & cos\lambda cos\phi & -cos\lambda sin\phi \\ -sin\zeta cos\lambda & sin\zeta sin\lambda cos\phi + cos\zeta sin\phi & -sin\zeta sin\lambda sin\phi + cos\zeta cos\phi \end{bmatrix} \tag{2.2}$$

$$\times \begin{bmatrix} cos\Phi cos\delta cos\omega + sin\Phi sin\delta \\ -cos\delta sin\omega \\ -sin\Phi cos\delta cos\omega + cos\Phi sin\delta \end{bmatrix}$$

Declination Angle,

$$sin\ \delta = 0.39795 cos[0.98563(N - 173)], N = day\ number \tag{2.3}$$

Hour Angle,

$$\omega = 15(t_s - 12)°, t_s \text{ is the solar time} \tag{2.4}$$

The three orientation angles can be referred as the Figure 2.10 illustrated below. This three orientation angles are φ, λ and ζ respectively. φ angle is the horizontal direction change, which is the angle change on the horizontal plane; λ angle is the angle change on vertical axis, the slight roll on

the side and ζ angle is the angle change on the reference axis which is the inclination or declination. In the (Chong, et al., 2009), these angles become a need as the manufacturing of the hardware prototype is not at the exact right alignment. Including these orientation angles improves the accuracy of the tracking error.

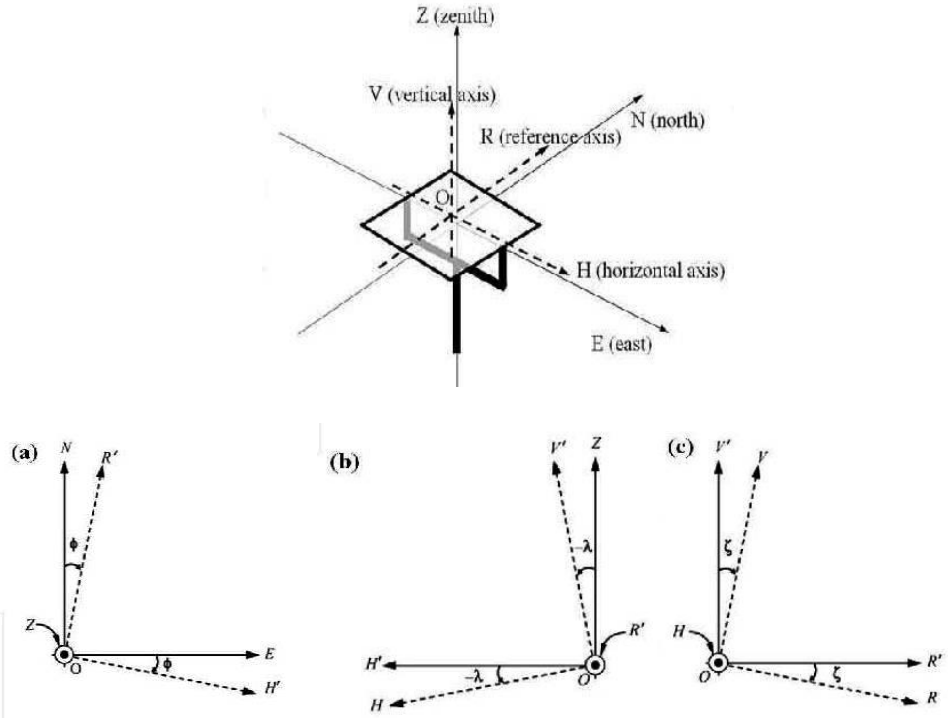

Figure 2.10 The three orientation angles (Chong & Wong, 2009)

2.4 Electric Vehicles

Vehicles are now playing important roles in our daily lives. Especially in developing countries such as Malaysia, self-owned vehicles are the essential tool for transportation in the daily life. As it is known that most vehicles in the past decades are all petroleum-based and have become one of the major sources of environmental pollutions. Replacing petroleum-based vehicles is

one of the effective ways to reduce carbon emission as well as dependence on fossil fuels; electrical vehicles (EVs) are then introduced to the market. EVs are introduced for quite a number of years, yet it is still not a popular choice, even though it is claimed to be two to three times more efficient than those which run on petroleum as internal combustion engines (Thomas, 2009) (U.S. Department of Energy, 2013). Furthermore, those stations which provide the electricity to the EVs are still using fossil fuels in many countries; this has created a stumbling block for EVs. Meanwhile, EVs are less popular as compared to normal petroleum car because of the less availability of the charging stations. We can resolve this problem if we have a design like a mini on-the-go power plant which we can use to recharge the EVs on the spot when their batteries run out of electricity; as long as the EVs have the exposure to the sun irradiation as suggested in our proposal. This would be a very attractive solution to boost the usage of EVs on the road as the mini on-the-go power can provide a better energy extraction throughput and car batteries can be charged anytime and anywhere even while travelling, given that it has the exposure to the sun irradiation. In other words, such design could boost the energy efficiency of vehicles by increasing the effective travelling distance, which means that the electricity can “re-supply” again as long as EVs have the exposure to the sun irradiation. Furthermore, if it is necessary for vehicles to travel to remote and barren area, this mini power on-the-go plant is handy to charge the vehicles and let the vehicles remains moving as well as promoting the economic activities in those areas. This concept can also apply to other transports such as trains, ships and etc. For example, if the system is applied on ships, it will be powerful secondary power source to sustain the system if it

is out of fuels upon emergency, enabling others to come into rescue without the loss of communications. Next, this mini on-the-go power plant would be a significant impact for those countries which suffer from shortage of land to build a large power plant. This system can come in handy and being installed anywhere.

2.5 Control System

The control system can be divided into PC (Personal Computer) based control system and micro-controller or microprocessor based system. These control system is used to control external connected hardware or peripherals that need periodic action or performing certain actions under certain criteria that is programmed on the control system. The controller is acting as the master brain based on different types of system designs. The control system is set or programmed to send the commands to the peripherals and let the peripherals to perform the action accordingly. For PC-based control system, the peripherals can be connected to the PC via serial port (RS-232) or the Universal Serial Bus (USB) port. While for microcontroller or microprocessor control system, the peripherals can be connected to the controller via USB, General Purpose Input Output (GPIO) port, SPI and I2C ports. PC-based control system usually is used on large sized system or static system while for microcontroller based control system usually is used on smaller sized system, automated, portable or mobile system.

There are a few types of microcontroller or microprocessor based control system, each of the microcontrollers has its own advantages as well as

disadvantages; also, the choice of microcontroller system is based on the system design criteria. In addition, the type of peripherals and connection type of the peripherals will affect the choice of the microcontroller to be used in the system design.

2.5.1 Android-based Control System

Smart phone is now very common and almost everyone would have one on hand. Depending on the model, the processors employed by most of the smart phones as the main controllers are from Broadcomm, Snapdragon or Quadcomm. The choice of OS of the smart phone that we are looking into is Android. In Android-based smart phone, user program is called application and for most of the applications it can be developed by using Java programming languages or Java scripts. For the application that needs to communicate with the sensors that pre-installed in the smart phone motherboard, native Java programming is needed. The microprocessor of the smart phone is powerful and it is capable to do mathematics calculation so it can be one of the choices of control system.

For most high-end or flagship smart phone, digital compass sensor is pre-installed and it could be used by the developers and users after writing a specific application to access the sensor but for middle-range to low-range smart phone, this sensor is not equipped. On the other hand, if the smart phone is used for a long period or had some direct physical damages, it would affect the digital compass sensor in the smart phone. The surrounding of the smart phone in use is also affecting the accuracy of the sensor. If the smart phone has

a lot of direct contact with metals or magnetic field interference, the readings of the digital compass would not be accurate.

Furthermore, Android based smart phone is fully embedded inside the casing, so to connect it with the hardware, it is either removing the casing and connecting the hardware to the motherboard directly or using another microcontroller as the interface between the Android smart phone and hardware of the mobile solar tracking system. Android based smart phone is not designed to directly control external hardware system, so it creates some unwanted issue or problem during the development. If developer needs to connect the hardware through Android on the motherboard, it will be involving the recompilation of kernel and Operating System (OS). This process can be said as customizing specific ROM for Android system. The process is complicated and it is not the main purpose of this study.

2.5.2 Arduino

A small microcontroller that could be powered by battery would be a good choice for the development of the mobile solar tracking system. Arduino is a small sized microcontroller and it can be programmed by using PC. Arduino itself is equipped with an IDE which can install on the PC and using embedded system programming language that almost similar to C programming language.

The advantage of Arduino is that it can connect to sensors or small integrated circuits (ICs) via the available ports on the board. Arduino can

support multiple hardware connection, such as I2C connection, SPI connection and GPIO connection. Breakout board designed sensors usually can be connected to Arduino easily via jumper wire on the hardware and for the software; there is a number of available libraries that can be used in the development. On the other hand, there is some external shield circuit which can attached directly above the Arduino main board to provide more thorough control for the developers, for example, SD shield and network shield. Arduino itself need not to re-open or re-run the program once after the written program is uploaded to Arduino board; meaning if the developer does not upload a new program, Arduino will run the previously uploaded program once it is booted up either by the USB power or 3.5 power jack.

Arduino is small and compact, so the processor is contrarily small compare to Android based smart phone. It is not capable to run complicated computation as the ram available for Arduino is also small. Arduino can work standalone but to trace or debugging which involving both hardware and software would be hard as the program need to be uploaded to Arduino main board but there is nowhere to debug after that as Arduino main board is not equipped with debugger inside.

2.5.3 Raspberry Pi

Raspberry Pi is also a microcontroller and it is only with a size of a credit card for most of its models. Raspberry Pi itself is a mini computer which is capable to be booted up and use like a normal PC but with a compact size and without a display interface. It has the HDMI port and a display port

which allows user to connect with either to monitor, TV screen or a 3.5 inch, 7 inch LCD display. Raspberry Pi is using Raspian OS and the monitoring and using of this OS is similar to most Linux OS. For Raspberry Pi, python programming language can be used and this programming language is capable to code the hardware controlling as well which is different from other system. Raspberry Pi holds the great advantage where it can be powered up by battery or any external power device with 5V and 2A with mini USB port but posses with the ability like a computer.

Raspberry Pi can works standalone and also allows users to connect external peripherals, breakout boards, ICs onto the predefined ports on the main board. Raspberry Pi available hardware connection ports is similar to Arduino but Raspberry Pi also built in with USB ports, which allows the peripherals that uses USB port to connect directly. Raspberry Pi itself has own storage and lots of built-in library, users can use it easily by programming a python code or can control directly by entering command on the terminal in Raspbian OS. On the other hand, Raspbian OS can be run in command mode or Graphical User Interface (GUI) mode. Raspberry Pi also allow user to autorun program after the system is booted up, like automation and user are free to interchange between the program to run just by changing the scripts that saved in Raspberry Pi. A microSD card is used as the storage of Raspberry Pi; the OS of Raspberry Pi is stored inside this external storage as well as user program or data. User can retrieve the data by saving it inside flash drive or modify any program easily by connecting Raspberry Pi to the display screen.

Raspberry Pi is still under development, so its processor speed is slower as compared to the Android-based control system. For the Raspberry Pi that currently use in this study, it does not included with a python debugger but any errors or warnings will still be shown by the compiler on the terminal.

CHAPTER THREE

METHODOLOGY

3.0 Methodology

There are several challenges to design and implement a complete prototype of a mobile solar tracking system. We design the dynamic solar tracking algorithm based on the General Formula of Sun Tracking (Chong & Wong, 2009). From the formula, several inputs are required to compute the trajectory angles of the sun. Local time, date, declination angles are the common variables in both mobile and non-mobile sun tracker design. On the other hand, variables such as geographical coordinates and orientation angles of the sun tracking system, which are constant in non-mobile solar tracking system but these parameters, are time-variant for dynamic solar tracking system on mobile platform. Geographical coordination of the mobile platform gradually changes as compared to that of non-mobile solar tracking system and therefore, a sensor is needed to detect the change of location from time to time to prevent calculation of rotational angles from using incorrect geographical coordination.

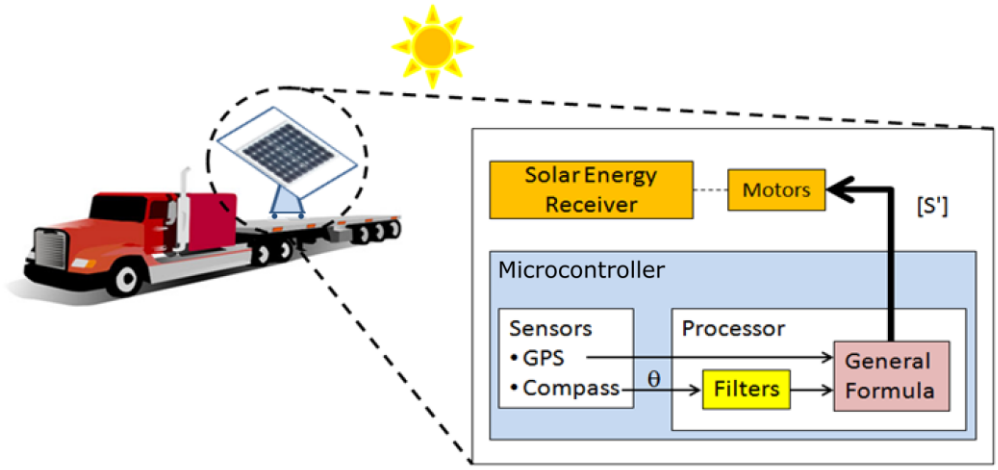

Figure 3.1 Illustration of the Mobile Solar Tracking System

Meanwhile, based on previous studies (Chong & Wong, 2009), we knew that the orientation angles of solar tracker would affect the calculation of the rotational angles. In the non-mobile solar tracker design, the orientation of the structure is often carefully measured and aligned to the axes based on each calculation of the angles of sun trajectory. While for mobile solar tracker design, it would be impossible to keep the mobile platform aligned to the few axes due to the road condition and also the route design. Among the orientation angles, heading angle, which is the moving direction of the mobile platform, is the angle which affects the most. The current quadrant of the mobile platform will affect the calculation of the rotational angles. In this non-mobile situation, the moving direction of mobile platform will not always face toward north; it will have the possibility of facing any direction such as east, west and south. In order to determine the current moving direction of the mobile platform, a digital compass sensor is necessary to identify the current heading angle with respect to north.

Sensors are necessary in the design of the dynamic mobile solar tracking system, but due to the sensitiveness of sensor, it is essential for us to further analyze before using it in the system. As we are using digital compass to determine the orientation angles of the mobile platforms, there would be some unwanted noise or machine errors. To get rid of these unnecessary noise and spikes, we designed and implemented a filtering algorithm to filter the noises and spikes to make sure the sun tracking activity run smoothly. As we are using a microcontroller to control the whole dynamic solar tracking system, we need to avoid burdening the memory and over-consuming the power of the microcontroller using highly complex algorithms; the filtering algorithm is preferable to be simple but effective to maintain the effectiveness of the dynamic mobile solar tracking system.

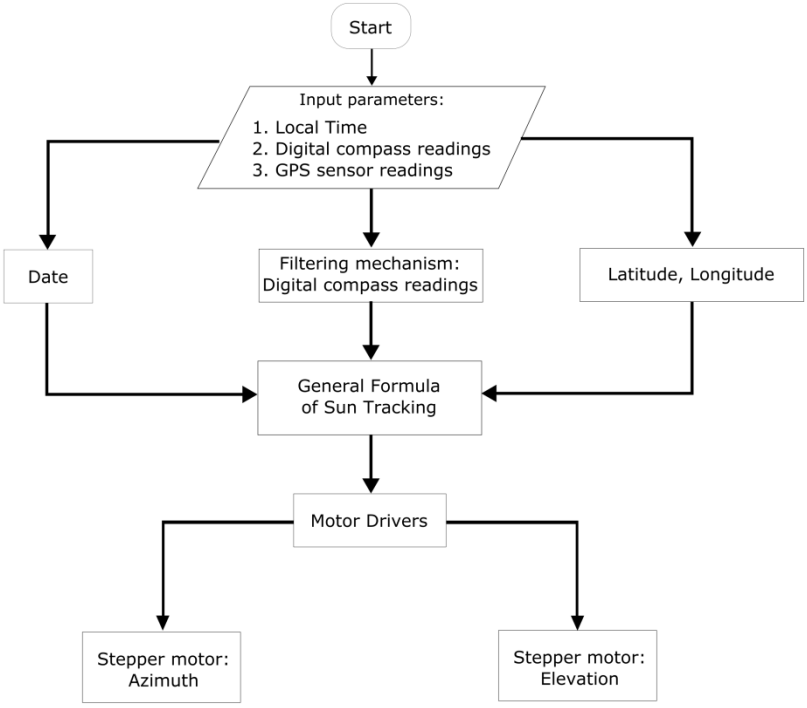

Figure 3.2 Flow Chart of Basic Flow of Mobile Solar Tracking System

For the calculation of the rotational angles, a work-alone microcontroller is used to perform the calculation. As illustrated in Figure 3.2, we can have any smart phone or work-alone microcontroller to serve as the “master brain” of the calculation. The “master brain” has to get all the parameters needed in the formula and then compute the rotational angles based on the given inputs; readings from GPS sensor and digital compass, system time then to the computation of the rotational angles. After getting the rotational angles, the microcontroller is able to compute the amount of steps needed for each motor to actuate the solar energy receiver to face the sun at the correct angle to receive maximum sun irradiance.

In non-mobile solar tracking system, it is possible for the solar tracking system to track the sun continuously. While for mobile solar tracking system, the continuous tracking might be a waste of energy because if the mobile platform is running on a straight path, we can reserve the energy for the actuation of solar energy receiver during the turnings or some other road condition; also, if the mobile platform is travelling on a bad road condition such as bumpy road or many holes along the path. The mobile solar tracking system is continuously monitored but it is not continuously tracking. The tracking criteria will be based on the timing control of the dynamic tracking mode which will be discussed later.

3.1 Mobile Tracking

3.1.1 Overview

In our studies, the main concern will be the mobility of the system as this system is to be designed to work on mobile platforms. To implement the mobile tracking, multiple sensors are included in the system to detect the environmental changes, including the change of route or path, the change of direction, the change of position and the condition of the road travelled. From the detection of the sensors, we can perform our computation based on the readings that we get from the sensors.

During the testing and implementation of the sensors, we identified some issues before finalizing the sensors to be used in the rest of the system design. The sensors been used throughout the testing and development of getting the heading direction are HMC5883L a magnetometer, combination of HMC5883L and MPU6050 which is magnetometer and accelerometer, Android-based smart mobile phone built-in compass and OceanServer OS-5000USD 3 Axis Digital Compass. These three types of digital compasses are tested in the experiments. The microcontrollers used during the implementation of the digital compass are Arduino, Android-based smart mobile phone and Raspberry Pi.

On the other hand, during the testing of each of the digital compass design, we found out that noises occur for all the digital compasses, although the digital compass is stationary. To maintain the efficiency and effectiveness of the mobile solar tracking system, we implemented a filtering algorithm to

get rid of unwanted noises from the readings of digital compass sensors.

The main focus of the mobile solar tracking system is the heading direction of the mobile platforms as the formula of calculating the rotational angles is very sensitive to quadrant change; also the change of the current position is very small as compared to heading direction. A GPS sensor is used to get the current position of the mobile solar tracking system. The choice of a GPS sensor depends on the type of microcontroller being employed; the main criteria has to make sure that the GPS sensor does not disturb the magnetic field around the compass by using minimum number of wires or connections to cut down the electromagnetic field across the system.

3.1.2 Dynamic Positioning

In the application of the dynamic solar tracking system on mobile platforms, variables have become functions of time rather than static constants. Referring to the application of General Formula of Sun Tracking (Chong, et al., 2009), geographical information like the latitude and longitude coordinates can be obtained by attaching a GPS sensor into the system. The GPS sensor will periodically detect the latest current location information and pass it to the formula to compute the rotational angles of the sun trajectory.

In our studies, the Bluetooth Garmin GLO GPS sensor is used to obtain the geographical information. This Bluetooth Garmin GLO GPS sensor uses Bluetooth serial communication to communicate with the microcontroller to cut down the possibility of wiring issue between the components and the

microcontroller. The specification of Garmin GLO GPS sensor is listed in Table 3.1.

Table 3.1 Bluetooth Garmin GLO GPS Sensor

Parameter	Value
Unit Size, W× H × D	1.78 × 4.19 × 7.72 (cm^3)
Weight	60.1 grams
Receiver Technology	GPS + GLONASS
WAAS	Yes
Update Rate	10 Hz
Accuracy	3 meters
Battery Capacity	1100 mAh
Battery Life	12 hours
Hot Start Time	3 – 5 seconds
Warm Start Time	35 seconds
Cold Start Time	60 seconds

The microcontroller that we are using throughout the design and development of the mobile solar tracking system is Raspberry Pi B+ model, which does not come with the built-in Bluetooth connection, so we attached an USB Bluetooth dongle to perform the connection between Raspberry Pi and the Garmin GLO GPS sensor. With the program in the microcontroller, the geographical information is read and passed for further computation.

3.1.3 Dynamic Heading Direction

On the other hand, the three orientation angles, φ, λ, ζ can be obtained by using a digital compass sensor. φ angle is the horizontal moving direction change, i.e. the moving direction of the mobile platform; λ angle is the angle change on vertical axis, the slight roll on the side and ζ angle is the angle change on the reference axis which is the inclination or declination. The horizontal moving direction, φ can also be translated as the current moving direction of the mobile platform, for example turning to right is with respect to turning from north direction to east direction. λ angle can be explained as the side rolling angle which should not vary much in normal working condition; but when the angle is big, it means the mobile platform has rolled over due to an accident. ζ angle indicates if the mobile platform is moving either uphill or downhill. These values will then be fed into the General Formula (Chong, et al., 2009) to calculate the unit vector of sun relative to the solar collector to adjust the pointing direction of the solar energy receiver. Figure 3.3(a), (b) and (c) illustrate the angle changes of φ, λ, ζ respectively.

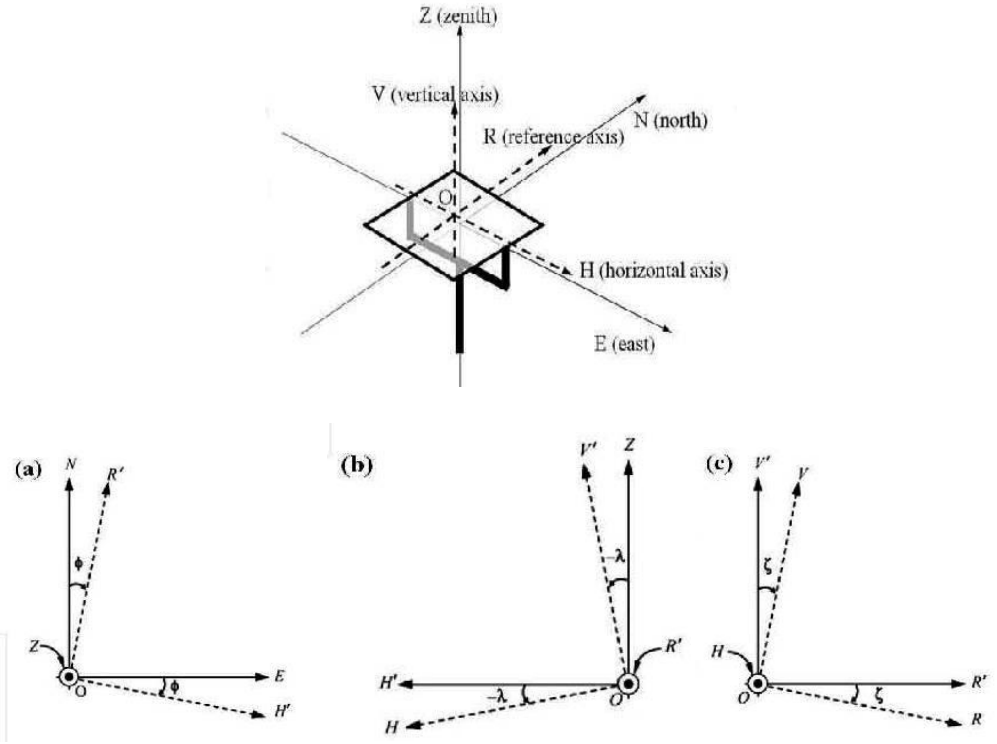

Figure 3.3 The three orientation angles (Chong & Wong, 2009)

The digital compass sensor is no longer uncommon and it now come in handy, they are also available as off-the-shelf portable gadgets at affordable cost. The moving speed of the mobile platforms will affect the precision of the GPS coordinate readings. From experiments, change of 1km in latitude and longitude only make a difference of ±0.2% to ±0.01% respectively in values for most of the GPS sensors (Lai, et al., 2014). From this we could said that the changes in the geographical coordinates of the mobile platforms are not fast enough to detect the logical difference in the calculation of the incident angle in the General Formula of Sun Tracking (Chong & Wong, 2009).

Based on the General Formula of Sun Tracking, we knew that the formula is sensitive to the quadrants as well as the moving direction of the mobile platforms. Although we can obtain the current geographical location of

the mobile platform by using the GPS sensor, it cannot determine which direction that the mobile platform is currently facing. It would be possible that at the mobile platform is facing east instead of north direction, which we could not tell from the GPS coordinate readings. As such, it is essential to use the digital compass in detecting the current moving direction of the mobile platform. Digital compass needs to calibrate angle with respect to real north of the mobile platform, so that the mobile solar tracking system is able to compute the accurate rotational angles to actuate the solar energy receiver.

The orientation angles have become functions of time as compared to the non-mobile system, we use $\theta(t)$ to symbolize moving direction change of mobile platform with respect to real north at the time, t with condition of$0° \leq \theta(t) < 360°$. This time function is generated based on the readings of the digital compass sensor in real time. The four common directions, north, east, south and west is corresponding to the four angles which are $\theta(t) = 0°, 90°, 180°$ and $270°$ respectively. The dynamic mobile solar tracking system can interpret the change from the reading of the digital compass and perform the correct calculation of the rotational angles.

There are three different implementations of the digital compass, which are HMC5883L, combination of HMC5883L and MPU6050, lastly OceanServer USD5000. In the very first implementation of the digital compass, we use only HMC5883L which is a magnetometer chip to detect the earth magnetic field. We used Arduino as the microcontroller to get the reading from the HMC5883L magnetometer from the I2C communication. We

have done stationary state experiment and also a small square route mobile experiment. From the data that we collected, the HMC5883L alone hardly can provide an accurate angle. A magnetometer is not enough to be an accurate heading direction sensing for our mobile solar tracking system. Only the magnetometer is not enough as we could not confirm that the magnetometer is at the exact alignments during the experiment or in use. Another sensor is needed to make as compensation to lead as a better heading direction guide. An accelerometer has to be added as the tilt-compensated function for the magnetometer. In the next experiment, this accelerometer sensor is added and worked together with magnetometer.

In the second implementation, we added MPU6050 to work together with the HMC5883L. The MPU6050 consists of two sensors, which is the gyro meter also the accelerometer. Gyro meter is to detect the degree of change but it is not useful for our system so the reading is ignored; only the reading of the accelerometer is used. The accelerometer can detect the pitch, yaw and raw; and with the HMC5883L three axes, x, y, and z readings, these six readings combines to get the heading direction readings. This is the same function as the tilt-compensated digital compass. We implemented it on Arduino as well and completed the set of experiments same as the first implementation.
Figure 3.4 Three axes of Magnetometer and Accelerometer

is the formula showing the implementation of both sensors to create a tilt-compensated digital compass. The three readings from the magnetometer can be denoted as MagnetomerX, MagnetometerY and MagnetometerZ with respect to the three readings from the x, y and z axes while the three axes readings from the accelerometer can be denoted as AccelerometerX, AccelerometerY and AccelerometerZ respect to the three axes readings from the x, y, and z axes (illustrated in Figure 3.4).

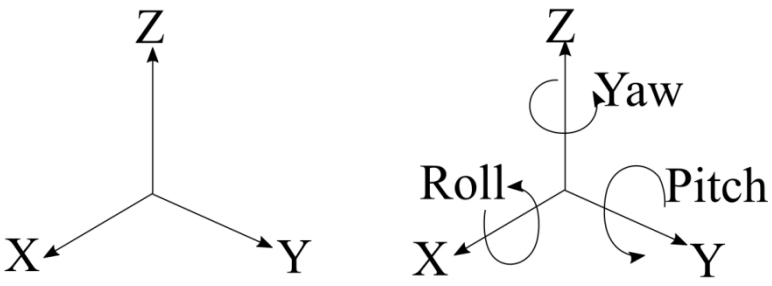

Figure 3.4 Three axes of Magnetometer and Accelerometer

Tilt-compensation of Digital Compass,

$$\boldsymbol{Roll = sin^{-1}(AccelerometerY)}$$

$$Pitch = sin^{-1}(AccelerometerX)$$

$$x = MagnetometerX \times cos(Pitch) + MagnetometerZ \times sin(Pitch)$$

$$y = MagnetometerX \times sin(Roll) \times sin(Pitch) + MagnetometerY \times cos(Roll) - MagnetometerZ \times sin(Roll) \times cos(Pitch)$$

$$\theta = tan^{-1}\frac{y}{x}, \theta \text{ is the heading angle} \quad (3.1)$$

Each time the Arduino get the six readings from two sensors, Arduino will be performing the computation and print out the computed reading, θ (Steps in

Tilt-compensation of Digital Compass). All of the data is stored in the SD card and the analysis will only perform after extracting the data from the SD card.

The study is focusing on mobile solar tracking system, we had written an Android application as most of the Android-based smart phone is provided with the magnetometer and accelerometer. During the experiments, we realized that if the smart phone is used for a long time or the mobile phone is dropped or having any physical damages, it can affect the reading and the reading could not stable down and keep fluctuating between $\pm 1°$ to $\pm 5°$.

Sometimes, the reading sometimes could vary for more than 10° on certain directions.

Finally, we found a 3-Axis digital compass from OceanServer, which is the OceanServer US500USD 3 Axis Digital Compass with USB connection. This 3-axis digital compass already implemented the tilt compensation and it can provide the readings with respect to the three orientation angles that we need in the computation of the rotational angles. The specification of the OceanServer US500USD 3 Axis Digital Compass is shown in Appendix 1.**Error! Reference source not found.**

This OceanServer digital compass connects to the microcontroller via the USB connection and detail of the connection communication is written in the software design. The microcontroller will read data from the digital compass and perform the extraction of the value readings before passing to the main algorithm to compute the rotational angles of sun trajectory.

During the implementation, we realized that there are lots of unexpected spikes and noises occurred in the readings of the digital compass; therefore, it made the development of a filtering algorithm essential to remove the spikes to perform a stable and effective tracking activity. Filtering algorithm will be discussed later.

3.2 Software of Mobile Solar Tracking System

3.2.1 Overview

As mentioned, the sensor that we used could have spikes or noises, so it would be essential for us to have a filtering algorithm to filter out these unwanted noises. For the software design, we are using Raspberry Pi as the main micro-controller to compute the calculation as well as controlling the hardware system. Raspberry Pi is chosen as it is stand-alone microcontroller and small in size while having onboard General Purpose Input / Output (GPIO) ports, SPI ports, USB ports, VCCs and so on which are capable to connect sensors or some small electronic circuits components. The sensors or electronic components can connect to Raspberry Pi via the ports that mentioned and Raspberry Pi could control any of them by using the function in the Python library. Sensors that we used in our design are digital compass from OceanServer as well as Bluetooth GPS sensor from Garmin. This OceanServer digital compass that we used is a 3-axis tilt compensated compass, is connecting to Raspberry Pi via the USB port. While for the Bluetooth GPS sensor, we attached a Bluetooth dongle on Raspberry Pi so that the GPS sensor can communicate with Raspberry Pi through the Bluetooth serial connection. Raspberry Pi itself is a small stand-alone micro-controller but it does not equip with clock crystal, so a Real-Time clock module is added to Raspberry Pi in order to extract the date and time from the system. On the hardware controlling, motor drivers are used as the interface between the stepper motors and Raspberry Pi. In the experiment to measure the tracking accuracy, a CCD camera is attached on the mobile solar tracker to capture the solar images during the solar tracking.

3.2.2 Noise Filtering

Among various types of filtering algorithms, we only considered simple algorithms as we need to avoid highly complexity algorithms that could consume significant power and take up the memory of CPU of the microcontroller that we used. Two simple algorithms are considered and studied; simple moving average (SMA) and simple linear regression (SLR). SMA is a function calculating the average of last m data of variable y; m can be denoted as the moving window size. If m is equal to 50, by using the SMA function, it will be calculating the average of last 50 readings that collected by the digital compass.

Simple Moving Average,

$$SMA = \frac{y_n + y_{n-1} + \cdots + y_{n-(m-1)}}{m}$$

$$SMA = \frac{1}{m}\sum_{i=0}^{m-1} y_{n-i} \tag{3.2}$$

The other filtering algorithm that used in our studies is SLR. SLR is least squares estimator of a linear regression model for modeling the relationship between a scalar dependent variable y and one independent variable x by fitting a straight line $y = \alpha + \beta x$ through the last set of m data. Below explained the α, β in the SLR algorithm that is used in our studies.

Simple Linear Regression,

$$\beta = r_{xy}\frac{s_y}{s_x};\ \beta = r_{xy}\frac{s_y}{s_x};\ \ni f = \alpha + \beta x \tag{3.3}$$

where, f: Straight line provides best fit for *m* data;

r_{xy}: Sample correlation coefficient between *x* and *y*;

s_x: Standard deviation of *x*;

s_y: Standard deviation of *y*.

In ideal case, $\theta(t)$ which is generated from the digital compass is the input to these two algorithms. Somehow, $\theta(t)$ becomes a discontinuous function when the mobile platform is heading north in practice because the actual readings of the digital compass is not a constant value $0°$ but a set of values oscillating between $(360° - \mu)$ and $(0° + \mu)$, whereby μ is the machine error of the digital compass. Since the function is not a continuous function, these algorithms do not work as we expected; the result of the average will become a number around 180º even though it is constantly pointing to real north. To obtain a correct input from the digital compass, we need to map these discontinuous readings into a continuous domain before doing the averaging. In this case, we considered using sinusoidal functions as they are continuous functions in nature. We take either cosine or sine functions of $\theta(t)$ as the inputs to apply to both of the filtering algorithms. The outputs of filtering algorithms are now more suitable compared to the raw values of $\theta(t)$. In the real implementation of the filtering algorithm, both sine and cosine needed to be used on different quadrant or else it will violate the purpose of our filtering process.

In our design, we use SLR to calculate the value of $f(t)$. It fits best within the outcome of the sinusoidal functions of the last *m* angles measured by the digital compass at the time *t*. SLR works well until there is a sudden change of angles occur in the original set of data. For SLR it would "overreact" in predicting the line that best fit for last *m* data, for example it predicted the value overshooting from the original data line. For some of the cases where sudden changes happened at the area around $\theta = 0°$ or $\theta = 180°$ where correspond to $cos\,\theta = 1$ or $cos\,\theta = -1$, it would be out of the ranges of the sinusoidal function, [-1, +1] which is no longer valid for sinusoidal function.

For SMA, it responds "slower" compare to SLR, whereby in our studies it lags "behind" our original data line which is opposite to SLR that runs "before" the original data line. SMA tends to smoothen the original data line and it has kept the approximating values remains in the maximum range of the sinusoidal function which is [-1, +1]. Since both of the algorithms have their own advantage and disadvantage, we have combining both of the algorithms together to create a compound filtering function, $F = \frac{SLR+SMA}{2}$ to create a better effect than just using either one of the filtering algorithm to calculate the collected data from the digital compass (Lai, et al., 2014). This compound filtering algorithm reduced the disadvantage of the SLR whereby it minimize the overreaction of SLR during the sudden change while speeding the SMA whereby it gives a faster approximation as compared to SMA alone. Both of these algorithms cover the disadvantage of the other algorithm where it creates a better solution for us and also combining both simple filtering

algorithms would not be adding too much computing power as compared to directly using a complex filtering algorithm.

3.2.3 Raspberry Pi and Communication between Peripherals

Figure 3.5 Communication between Raspberry Pi and Peripheralssimply showed the way of communication between Raspberry Pi and the peripherals. The communication used are IIC or I2C (Inter-Integrated Circuit), Bluetooth Serial communication, GPIO and USB Serial communication. OceanServer digital compass is connecting to Raspberry Pi via the USB port, so it is using the USB serial communication while Bluetooth GPS sensor is connecting to Raspberry Pi via the Bluetooth dongle that we attached to the Raspberry Pi, so it is using the Bluetooth serial communication. For the Real-Time clock module, it connects to Raspberry Pi via the I2C connection. Lastly, the motor drivers are connected to Raspberry Pi via the GPIO ports and motor drivers will respond to the pulses that send out from Raspberry Pi.

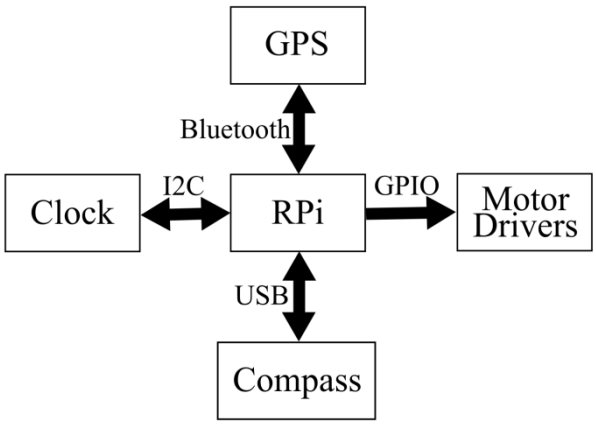

Figure 3.5 Communication between Raspberry Pi and Peripherals

3.2.4 Raspberry Pi and Digital Compass

Raspberry Pi is programmed to communicate with the digital compass at the baud rate of 9600 via the USB serial communication. In our design, data are captured at the rate of 30 readings per second. The readings from the digital compass and GPS coordinates are needed before each computation of the Azimuth and Elevation angles. After Raspberry Pi successfully collected the readings from both sensors, it can proceed to the calculation of the rotational angles. Before they are passed to the General Formula, we used the filtering algorithm that we developed to filter out the noises and spikes as those unwanted noises might cause excess solar tracking activity, wasting the computation power of Raspberry Pi as well as the power of the battery to actuate the solar energy receiver.

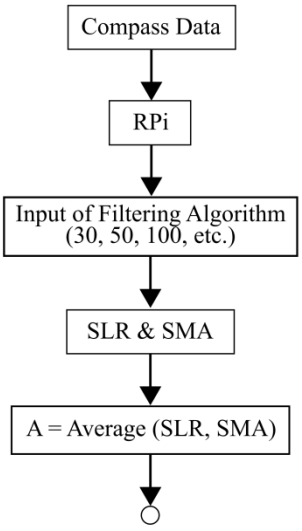

Figure 3.6 Flow of Data Acquisition step

The flow chart in Figure 3.6 shows the processing steps after collecting

readings from the digital compass sensors. For the inputs of the filtering algorithms, we can have 30, 50 or 100 moving size per calculation, depending on the condition during the solar tracking activity. For the larger window size, it can achieve better smoothing effect, but the response is lagging behind; while for small window size, the smoothing effect is not significant enough. An optimal window size is needed for the optimum solar tracking activity. Three sets of readings, which respond to three different orientation angles captured by digital compass, are filtered using the compound filtering algorithm before being passed to the General Formula to compute the Azimuth and Elevation angles.

3.2.5 Computation of Azimuth and Elevation Angles

After the process of sensors' data acquisition and applying the filtering algorithm, all the inputs that required by the General Formula is ready to use. They are latitude angle (Φ) from GPS sensor, hour angle (ω), declination angle (∂), time zone and three filtered orientation angles (ϕ, λ, ζ). If current time is 1st August 2017, 11:42:43a.m., time zone is +8.00, latitude is 3.1218, longitude is 101.9134 and three orientation angles are 127°, 1° and 2° respectively. The result Azimuth and Elevation angles are denoted as α and β respectively.

Getting Declination Angle,

$$sin\ \delta = 0.39795cos[0.98563(N - 173)], \qquad N = day\ number \qquad (2.3)$$

$$\rightarrow sin\ \delta = 0.39795cos[0.98563(213 - 173)]$$

$$\sin \delta = 0.3073982005$$

$$\delta = \sin^{-1} 0.3073982005 = 17.9°$$

$$\omega = 15(t_s - 12)°, t_s \; is \; Solar \; Time \tag{2.4}$$

$$\omega = 15(10.38866667 - 12)°$$

$$\omega = -24.17°$$

Substitute all the inputs into the formula,

$$[S'] = [\zeta][\lambda][\phi][\Phi][S] \tag{2.1}$$

$$\begin{bmatrix} sin\alpha \\ cos\alpha sin\beta \\ cos\alpha cos\beta \end{bmatrix} = \begin{bmatrix} cos\zeta & 0 & sin\zeta \\ 0 & 1 & 0 \\ -sin\zeta & 0 & cos\zeta \end{bmatrix} \times \begin{bmatrix} cos\lambda & -sin\lambda & 0 \\ sin\lambda & cos\lambda & 0 \\ 0 & 0 & 1 \end{bmatrix}$$

$$\times \begin{bmatrix} 1 & 0 & 0 \\ 0 & cos\phi & -sin\phi \\ 0 & sin\phi & cos\phi \end{bmatrix} \times$$

$$\begin{bmatrix} cos\Phi & 0 & sin\Phi \\ 0 & 1 & 0 \\ -sin\Phi & 0 & cos\Phi \end{bmatrix} \times \begin{bmatrix} cos\delta cos\omega \\ -cos\delta sin\omega \\ sin\delta \end{bmatrix} \tag{2.2}$$

$$\begin{bmatrix} sin\alpha \\ cos\alpha sin\beta \\ cos\alpha cos\beta \end{bmatrix} = \begin{bmatrix} cos2° & 0 & sin2° \\ 0 & 1 & 0 \\ -sin2° & 0 & cos2° \end{bmatrix} \times \begin{bmatrix} cos1° & -sin1° & 0 \\ sin1° & cos1° & 0 \\ 0 & 0 & 1 \end{bmatrix}$$

$$\times \begin{bmatrix} 1 & 0 & 0 \\ 0 & cos127° & -sin127° \\ 0 & sin127° & cos127° \end{bmatrix} \times$$

$$\begin{bmatrix} cos3.1218° & 0 & sin3.1218° \\ 0 & 1 & 0 \\ -sin3.1218° & 0 & cos3.1218° \end{bmatrix} \times \begin{bmatrix} cos17.9° \cos(-24.17°) \\ -cos17.9° \sin(-24.17°) \\ sin17.9° \end{bmatrix}$$

$$\begin{bmatrix} sin\alpha \\ cos\alpha sin\beta \\ cos\alpha cos\beta \end{bmatrix} = \begin{bmatrix} -0.960342 \\ 0.249875 \\ 0.123713 \end{bmatrix}$$

$$\alpha = 286.19°, \beta = 63.66°$$

3.2.6 Timing Control of Dynamic Tracking

For active tracking, the system is calculating the rotational angles based on the current time and location's data. It is tracking the Sun by the mathematical formulae. In non-mobile solar tracking system, it is applicable to continuously tracking the sun without any orientation issue as the system is remained at the same local position and the orientation is fixed after cemented on the location. While for mobile solar tracking system, position and orientation of the system is continuously changing during mobile state, so it would be hard if to remain the tracking activity continuously as they are changing gradually. Too often changes in the hardware would increase the difficulty of getting the solar energy receiver to point to the correct trajectory angles even though software can calculate the responding trajectory angles. Two modes are considered in this project, which are Time Lapse mode and Actuation Angle modes.

In time lapse (TL) mode, calculation and actuation loop is performed periodically with a constant time interval, t_L. The actuation of both motors is performed after the result of the calculation of the latest Azimuth and Elevation angles is done. Figure 3.7 illustrates the control flow of TL mode.

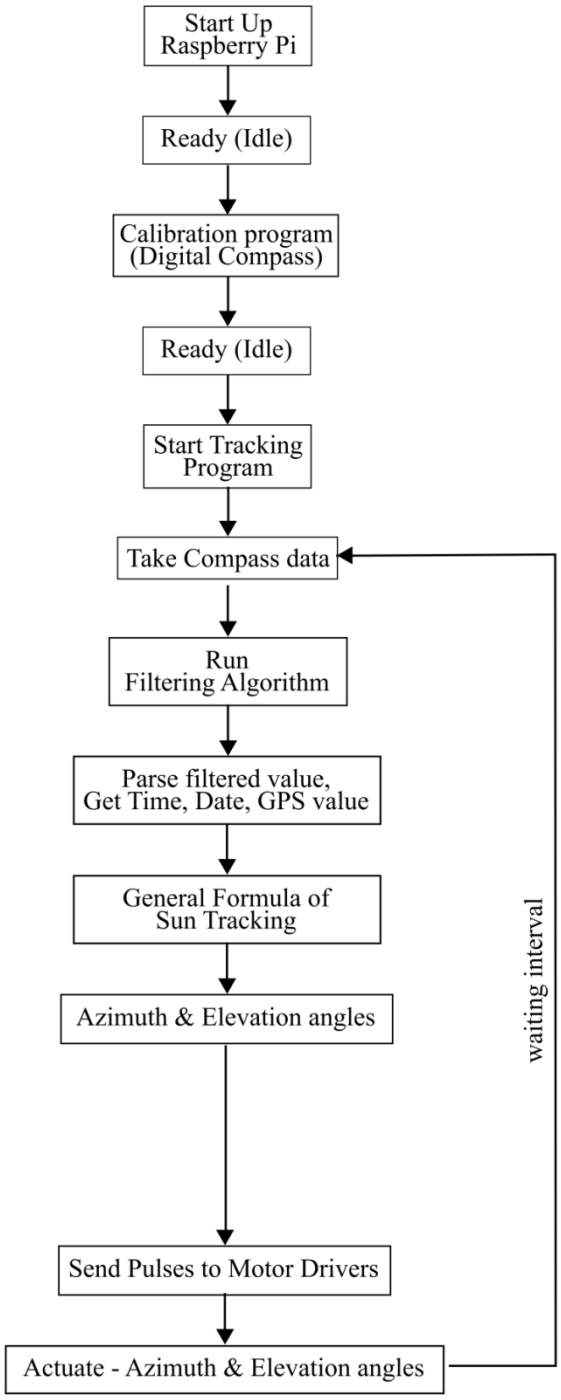

Figure 3.7 Flow of Time Lapse (TL) mode

Data acquisition from the digital compass and GPS sensor is performed after the start of the dynamic solar tracking program. Filtering algorithm and

the calculation of the rotational angles, Azimuth and Elevation angles is done right after the inputs needed are collected by the Raspberry Pi. The calculated Azimuth and Elevation angles will then be converted to digital pulses and sent to motor drivers to trigger the actuation. After actuating the solar energy receiver to the latest Azimuth and Elevation angles, the system will wait until the current t_L expires before the next round is started. The time lapses that we used in the experiments are 1 minute, 2 minutes and 5 minutes.

If the actuation only performed after certain criterion is met, it is called the Actuation Angle mode in this study; two feasible options are the Azimuth Actuation Angle (AZ) mode and Elevation Actuation Angle (EL) mode. AZ mode and EL mode have the similar criteria, but the main component is different. In AZ mode, we observes the change of the calculated Azimuth angle while in EL mode, we observes the change of the calculated Elevation angle. Azimuth angle can be explained as the horizontal change of the rotational angle of sun trajectory and Elevation angle is the vertical change of the rotational angle of sun trajectory. Horizontal change is obvious, such as changing angles or turnings but vertical change is less likely to have, like going uphill and downhill consecutively. For the EL mode, it is less likely to happen in Malaysia, as the coverage of the uphill and downhill roads are too less to be considered as common case in Malaysia, so we do not include any details about it; instead, we focus only on the AZ mode. The idea behind AZ mode is we only actuate the motors when the difference of newly calculated Azimuth and the previous actuated Azimuth angle exceeds certain desired threshold value. The threshold value that we used in experiments is 0.1^o and

0.5º. Referring to the flow chart in Figure 3.8, data acquisition, filtering and calculation of rotational angles will keep on looping until the threshold of the AZ mode is met; in our studies, when the calculated difference is equal or larger than the threshold, then it will trigger the motor drivers to perform the actuation and update the solar energy receiver to the latest correct position. After the actuation, the system will go back to the data acquisition step and continue with the consecutive steps.

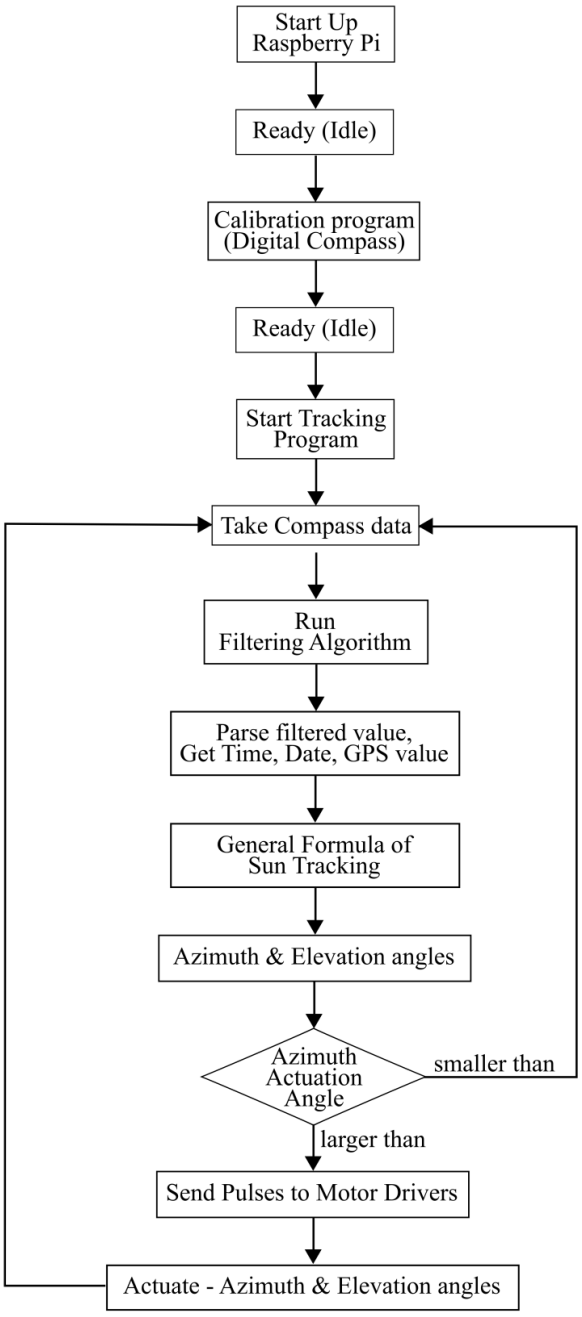

Figure 3.8 Flow of Azimuth Actuation Angle (AZ) mode

In the TL mode, if within the waiting period, the system will not do anything after the completion of actuation unless it is interrupted by the user,

for example pressing the stop button to end the solar tracking activity. After the waiting period, the system will go back to data acquisition step to collect the compass data and the algorithm flow will be repeating in the loop again. This approach is simple and the Raspberry Pi does not consume too much computing power. However, the actuation could be too frequent resulting in more motor activities and power consumption and potentially lower angle accuracy.

In the AZ mode, for every calculated Azimuth angle, the system will have a decision making step before sending the pulses to actuate the motors. The actuation will only be performed when the actuation criteria are met. Even though this mode is more complicated as compared with TL mode, this mode avoids unnecessary motor activities and waste of actuation power, at the cost of more computing power.

Figure 3.9 shows the side-by-side comparison of both timing control modes in term of the steps that both taken in flow chart form. The significant differences are flow in the motor actuation step and also the looping condition. For TL mode, it only takes care of the waiting interval, whenever the waiting interval is fulfilled only the loop will start again from data acquisition until the motor actuation step. There is no any decision making step taken throughout the whole system. While in AZ mode, there is an extra decision making step whereas it decides the actuation of the solar energy receiver in the motor actuation step. If the calculated Azimuth Actuation Angle is larger than the threshold, then the system will trigger the hardware actuation, while Azimuth

Actuation Angle is smaller than the threshold, the system will go back to the data acquisition step and recalculate the Azimuth and Elevation angles based on the latest collected inputs. No hardware actuation until the Azimuth Actuation Angle is fulfilled to be larger than the threshold, or else the system will keep calculating the latest Azimuth and Elevation angles.

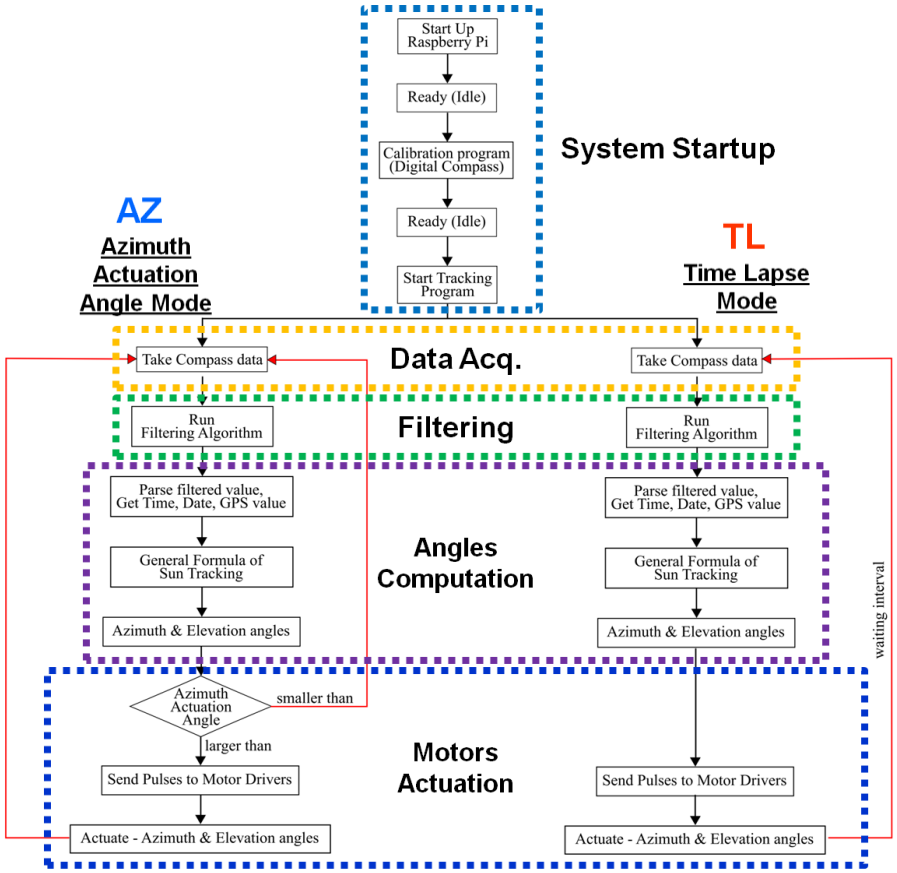

Figure 3.9 Comparison of steps in both Timing Control modes

If compares TL mode with AZ mode on the same time line and shows that the detection of angle changes tends to be more frequent in the AZ mode than in the TL mode. AZ mode keeps on calculating to check if the criteria are met while TL mode will just update the hardware of mobile solar tracking system after calculation of the Azimuth and Elevation angles. On the other

hand, TL mode is straightforward, as long it fulfill the timing interval, Raspberry Pi will send out the pulses to the motor drivers no matter how small the angles needed to be actuated are while for AZ mode, Raspberry Pi need to decide whether the motors need to be actuated before sending out the pulses to the motor drivers.

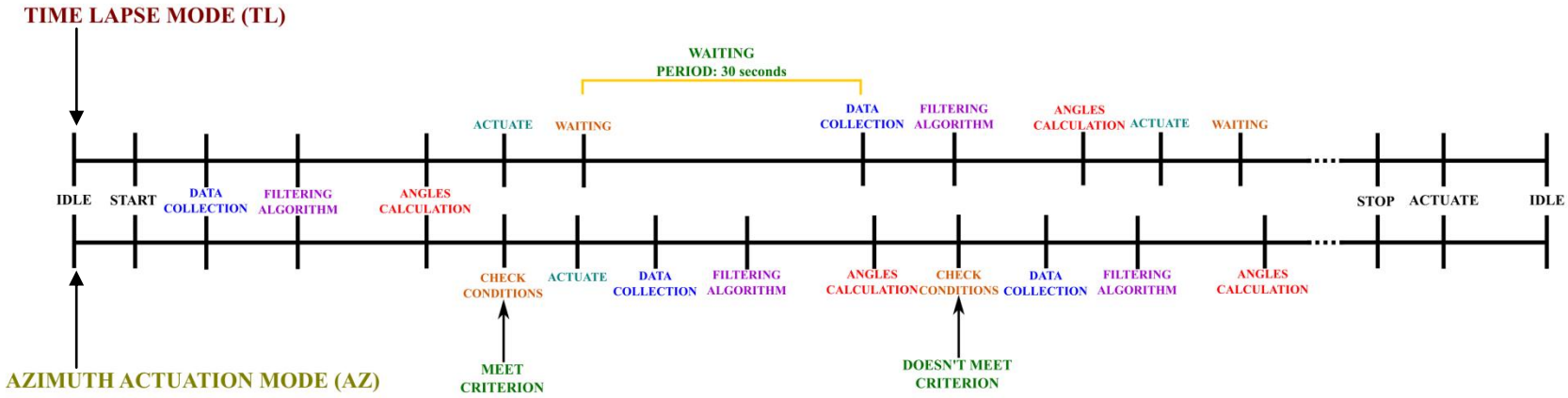

Figure 3.10 Comparison of both Timing Control mode in Dynamic Control

3.2.7 Motor Actuation and Compensation

The motor driver serves as the interface between the microcontroller and the motor, making the actuation of the motor simple and the entire microcontroller needs to do are the calculation of the required number of pulses and sending them to the motor driver.

Motor that chosen to be used in this mobile solar tracking system is stepper motor. Stepper motor coupled with motor driver enable user to control via motor driver to simplify the user's system. Stepper motor responds to user from the pulses received from motor driver. Motor driver receives the control from microcontroller to the motor. The control command that motor driver receives are number of steps and direction of steps. The speed of the actuation is controlled by the microcontroller, so it is not related to the any control in the motor driver. In 1-pulse mode, the motor driver receives only one pulse, which is the number of steps to actuate and either one direction will be applied throughout the entire usage. While in 2-pulse mode, the motor driver receives two pulses from controller. One is direction pulse, another is number of steps.

In our studies, motor actuation can go in both directions, i.e. clockwise and anti-clockwise, so the two pulses that we will be sending to the motor driver from the microcontroller are angles and directions. Two directions are used in our studies because if we are using one direction only, if the angles need to be actuated is more than 180º, for example, 290º, for only one direction case, the motor need to actuate from 0º to 290º, that is very time consuming and we need to avoid using too much of time actuating the motor

also this lags the whole system. If the same scenario in the two direction case, the motor is actuating from 360º to 290º, with the anti-clockwise direction, the angle that need to be actuated by the motor now is only 70º. Obviously, actuating smaller angle is using lesser time and it will consume less power in actuating the motor; also for our studies, the response of the update of Azimuth and Elevation angles need to be quick especially during the mobile state, or else the system will always be lagging away from the exact sun trajectory.

The angle needs to be converted to steps before sending it to the motor driver. In our studies, one single step of the motor applied in the mobile solar tracking system equals to 0.0144º. For example, 25º = 1736.1111 steps. Depending on the calculated rotational angles, if the angle is less than 180º, the pulse direction that the microcontroller sends is clockwise while if the angle is more that 180º, the pulse direction that the microcontroller sends is anti-clockwise. For the latter scenario, for example, if the angle needs to be actuated is 310º, the direction pulse will be anti-clockwise and the angle is $360° - 310° = 50°$. 50º is equal to 3472.2222 steps. The microcontroller will be sending 3472 steps and anti-clockwise pulse to the motor driver.

For the motor and motor driver, $1\ step = 0.0144°$, so if less than 1 step or less than 0.0144º, the remainder will be ignored by the system as the motor driver only takes integer number pulse. From the previous example, 3472.2222 steps, the motor driver only takes 3472 as the step pulse and the remaining 0.2222 step will be ignored. If this situation keeps happening, the

system will gradually drift away from the correct angle after some times. The solution we employed accumulates these small errors and compensates them to the next actuation in one lump sum as soon as the lump sum is greater than 1 step. Continuing from previous example, if the next actuating angle is 5.2º, the steps will be $5.2° \div 0.0144° = 361.1111$ steps. From the previous one is having a 0.2222 step remainder and newly calculated is having a 0.1111 step, here it will be accumulated a 0.3333 step remainder. If this situation continues, the hardware will be away from the actual calculated rotational angles, so the microcontroller keeps summing up the remainder angles that are less than 1 step until the lump sum eventually gets greater than 1 step.

shows how the motor step compensation is carried out in our system.

Motor Actuation with Compensation,

$$50° \div 0.0144° = 3472.2222\ steps \cdots (1st\ angle)$$

$$Remainder\ 0.2222\ step = 0.00319968°$$

$$Brought\ forward\ new\ angle, 5.2° + 0.00319968°$$

$$= 5.20319968° \cdots (2nd\ angle)$$

$$Steps, 5.20319968° \div 0.0144° = 361.33331111\ steps$$

$$Remainder\ 0.33331111\ step = 0.00479968°$$

$$Brought\ forward\ new\ angle, 3.7° + 0.00479968°$$

$$= 3.70479968° \cdots (3nd\ angle)$$

$$Steps, 3.70479968° \div 0.0144° = 257.277756\ steps$$

$$Remainder\ 0.277756\ step = 0.00399968° \quad (3.4)$$

Motor Actuation without Compensation,

$$50° \div 0.0144° = 3472.2222\ steps \cdots (1st\ angle) \quad (3.5)$$

$$Remainder\ 0.2222\ step = 0.00319968°$$

$$New\ angle, 5.2° \cdots (2nd\ angle)$$

$$Steps, 5.2° \div 0.0144° = 361.11111\ \ steps$$

$$Brought\ forward\ Remainder,$$

$$0.2222\ step + 0.1111\ step = 0.00479952°$$

$$New\ angle \leq ,3.7° \cdots (3nd\ angle)$$

$$Steps, 3.7° \div 0.0144° = 256.94444\ steps$$

$$Brought\ forward\ Remainder$$

$$0.3333\ step + 0.94444\ step = 1.27774\ step = 0.0183995°$$

In the situation without compensation, the remaining "un-actuated" angle will only accumulate and grow larger. In the contrary, the remaining "un-actuated" angle of the mobile solar tracking system can be always kept below 1 step which equals to 0.0144º with compensation; hence, theoretical tracking error is manageable and minimized.

3.2.8 Raspberry Pi and Solar Images

To study the accuracy of the proposed algorithm, CCD camera is installed in our mobile solar tracking system to capture the solar image during the tracking activity. It replaced the optical part of the hardware, which is the CPV system consisting the Fresnel lens and dielectric filled cross compound parabolic concentrator (CCPC) combination with the dark blue colored glass

paper layers and CCD camera. The dark blue colored glass paper is set up to 64 layers to prevent the overexposure during the solar tracking activity. A cross is placed on the center point of top box on top of the glass paper layers; the intersection point of the cross is acting as the center point reference in the solar image that we captured during solar tracking activity. CCD camera is attached right below of the protecting layer. The reserved hole that allowed sunlight to pass through is where the CCD camera is allocated. It is programmed to capture each solar image with the resolution of 1920 × 1280 pixels and according to the actuation mode that we set depends on the experiments.

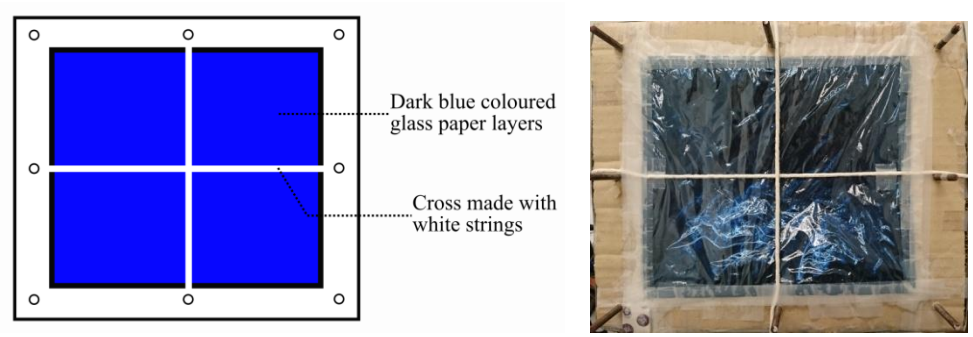

Figure 3.11 Glass paper layers and the position of cross (Illustration and Application)

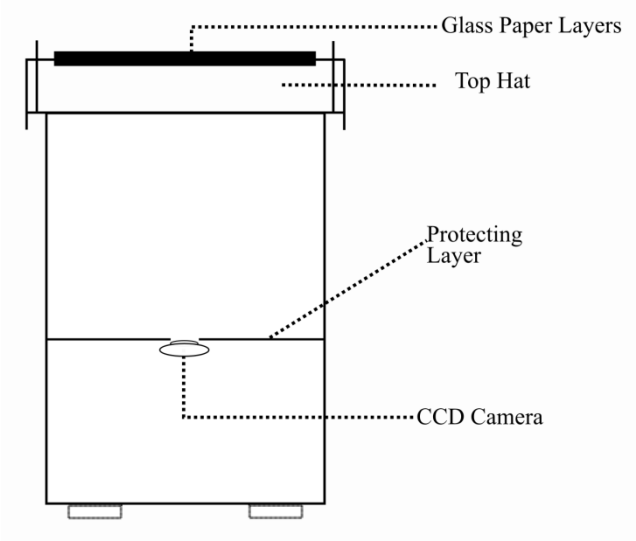

Figure 3.12 Position of the CCD camera inside the top box

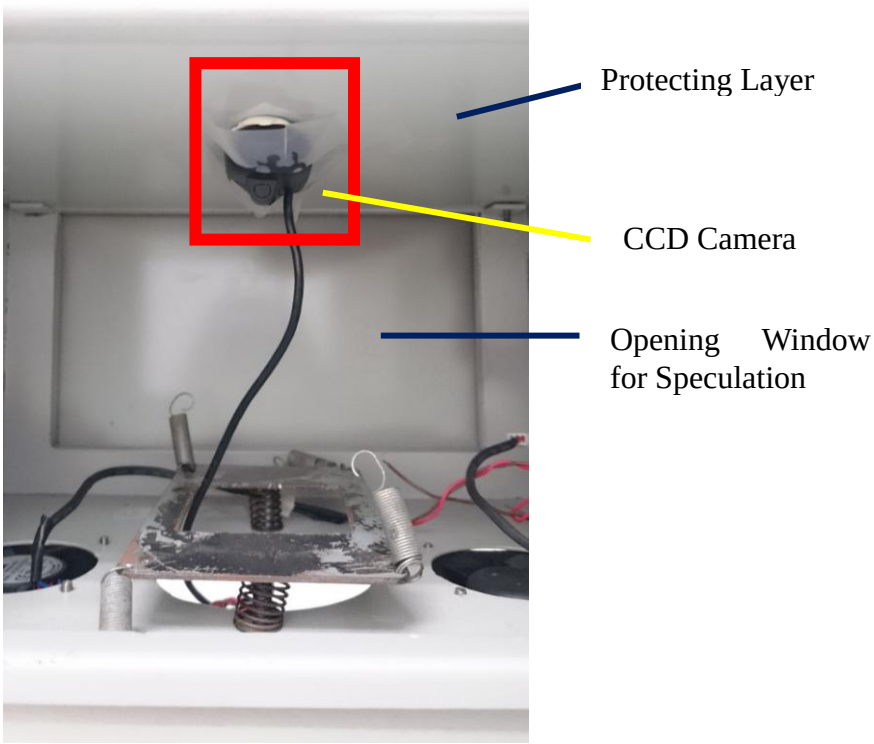

Figure 3.13 CCD camera attached at the bottom of protecting layer (Inside of top box)

Based on the two modes that we studied, timing for capturing the solar images will be different. For TL mode, solar image will be captured right after

the actuation of hardware. For AZ mode, solar image will be captured also right after the actuation and after each calculation of Azimuth and Elevation angles no matter the system triggers the actuation of the hardware or not. The solar images are extracted from Raspberry Pi after the experiment is done.

3.3 Hardware of Mobile Solar Tracking System

A prototype is designed and built in order to test out the algorithm of dynamic solar tracking. In this dynamic mobile solar tracking system, two special components are added, which is different from the non-mobile solar tracking system, are digital compass as well as the GPS sensor. Meanwhile, we need to consider the mobility of each component, such as the microcontroller, power source for motors and so on. With such, there are some constraints that need to be considered and evaluated before put all the hardware together. The design of this prototype can be separated into two portions, top portion consists of mechanical and optical parts and bottom portion is the controlling panel. Figure 3.14 shows the sketch of the mobile solar tracking system design.

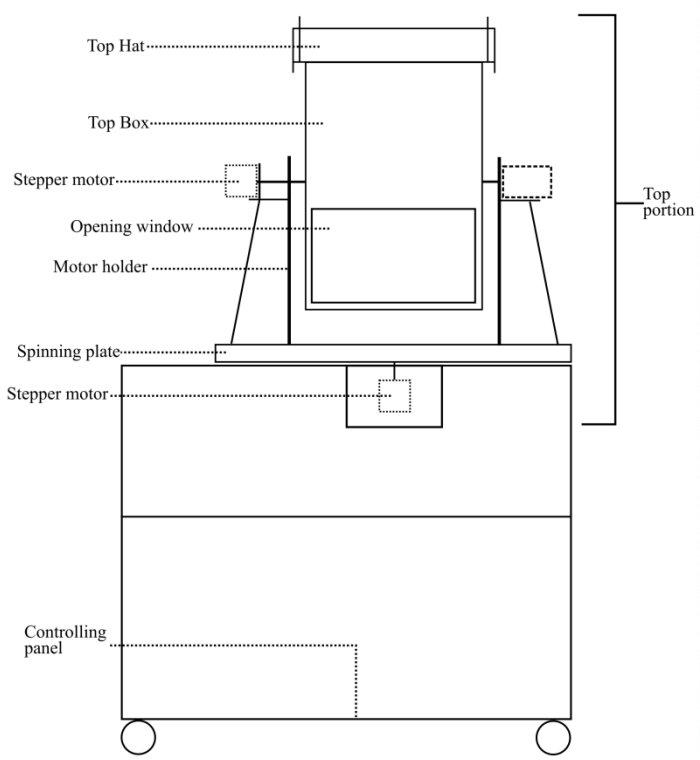

Figure 3.14 Skeleton Sketch of Mobile Solar Tracker design

Figure 3.15 Prototype during stationary experiment

Figure 3.16 Prototype attached on truck before starting experiments

3.3.1 Top Box

Top portion consists of two parts, mechanical as well as the optical part. On the mechanical part, we had an acrylic made “top hat” (Figure 3.17) as a holder for the first level of concentration. The design of the “top hat” has included the adjustable mechanism to allow easy calibration for different purposes and maintenance of Fresnel lens as well as also monitoring of the tracking activities while the system is running. The remaining part of the top

portion is the top box which is made of metal; the basic outlook is illustrated Figure 3.17. Material for second level concentration, solar cell and cooling system are all install in the top box portion. The top box is the solar energy receiver and in our studies, we need to make sure it is always aligned towards the Sun, allowing the maximum sunlight to focus onto our CPV system.

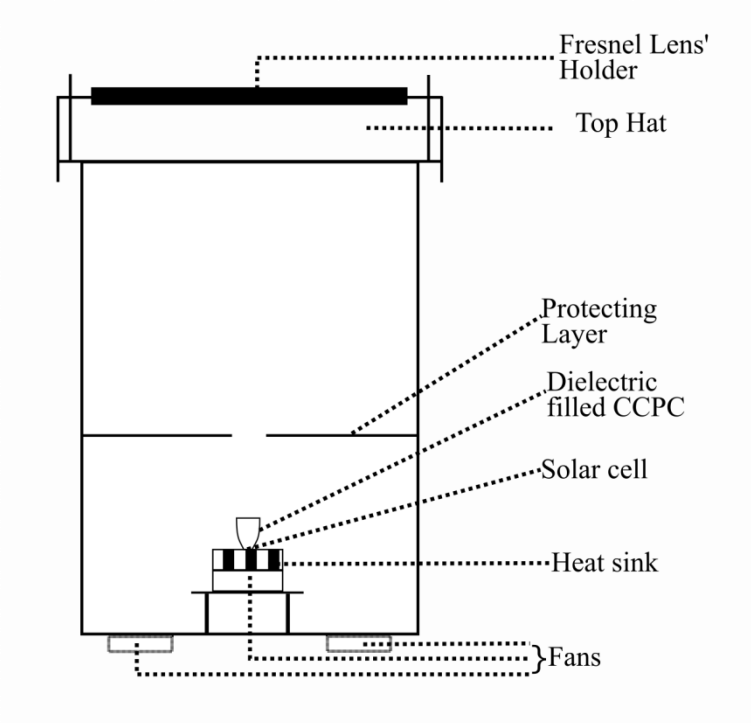

Figure 3.17 Top Box and its components

3.3.1.1 CPV System

The optical part of the hardware of the mobile solar tracking system consists of a two-level concentration system. First-level concentration is done by using Fresnel lens while the second level concentration is done by a dielectric CCPC. The size of Fresnel lens that we used in our study is 215.9mm × 266.7mm and the effective focal length is 457.2mm. During the

calibration and implementation of the first-level concentration, we fixed the Fresnel lens at the effective focal length, resulting the concentrated sunlight is a small point but falling onto other area that we are not expecting. This resulting point is of high in temperature and burns the pointing area in seconds. It become essential to protect other components inside the top box portion to avoid components being melted before it is put into use. To overcome this circumstance, we had a protecting layer installed right before the concentrated sunlight reaches the solar cell. This is to prevent the concentrated sunlight from falling on other area rather than the specifically designed area if any unexpected misalignment occurred during the calibration of hardware or tracking activities. There are a few openings designed for this protecting layer; one is the square opening for the first level concentrated sunlight to pass through, two rectangular openings on both sides are to keep the air-circulation for the cooling system of whole CPV system as illustrate in Figure 3.18.

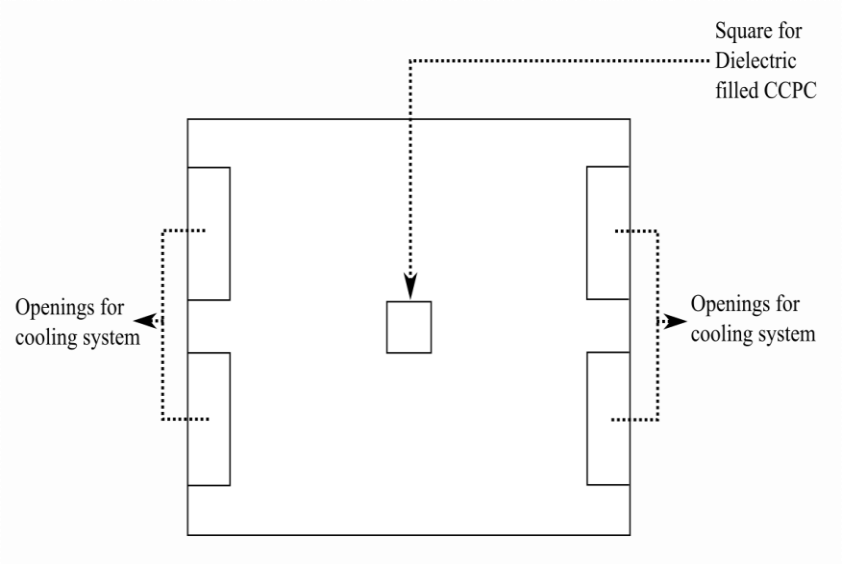

Figure 3.18 Openings in the Protecting Layer

.

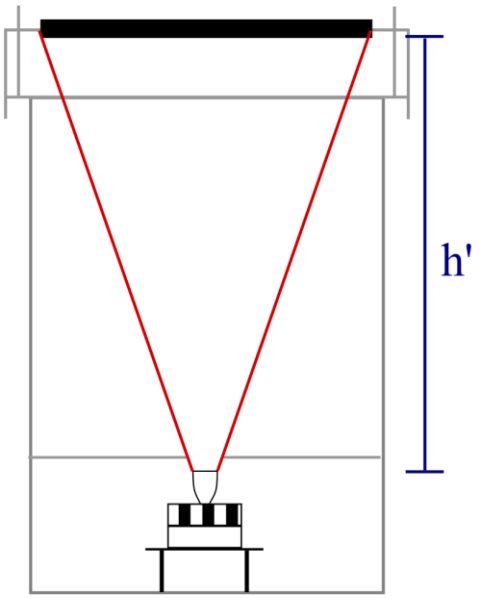

Figure 3.19 The height between Fresnel lens and Dielectric CCPC

As illustrated from the Figure 3.19, the distance between Fresnel lens and dielectric is calculated before designing the hardware of mobile solar tracker; based on the size of the Fresnel lens and dielectric filled CCPC that we are using. Based on the worst case scenario, the resultant image from the Fresnel lens, as the input of second level concentration should fully cover the top of the dielectric filled CCPC. From the calculation, we had the distance between the Fresnel lens and dielectric CCPC at 40.408 cm, the protecting layer is at 15 mm away from the CCPC and the opening hole reserved for the sunlight to pass through is 32mm × 32mm. If any misalignment occurs, the concentrated sunlight is less likely to reach any parts below the protecting layer. Side openings are required to promote the air circulation above the protecting layer as the internal of top box is at temperature up to 80ºC during the tracking activities. The cooling system and air circulation are very essential as high temperature will decrease the efficiency of the solar cell.

Calculation of h',

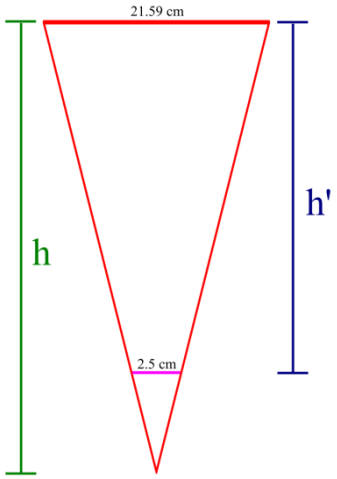

$$Width\ of\ Fresnel\ lens: 21.59\ \text{cm}$$

$$Width\ of\ Dielectric\ CCPC: 2.5\ \text{cm}$$

$$h = 457mm = 45.7cm, Effective\ focal\ length\ of\ Fresnel\ lens$$

$$\therefore h: 21.59 = (h - h'): 2.5 \tag{3.6}$$

$$\frac{h}{21.59} = \frac{h - h'}{2.5}$$

$$2.5h = 21.59(h - h')$$

$$21.59h' = 21.59h - 2.5h$$

$$h' = \frac{19.09h}{21.59}$$

$$h' = \frac{19.09 \times 45.7}{21.59}$$

$$h' = 40.408cm$$

At the best case scenario, the dielectric filled CCPC provides a tolerance for the first level concentrated sunlight, especially during the

tracking activities on mobile platforms. The tolerance given by the dielectric CCPC can be calculated as below. The measurement of the dielectric filled CCPC is 25 mm × 25 mm. The blue dots in Figure 3.20 show the furthest error tolerance points. To calculate the length from the center point to the blue dots, we can use the red line to calculate it. The top of the dielectric filled CCPC is a square, if we draw a line between two diagonal points (illustrated in Figure 3.20, the red line), named line c, which separated the square into two right-angle triangular.

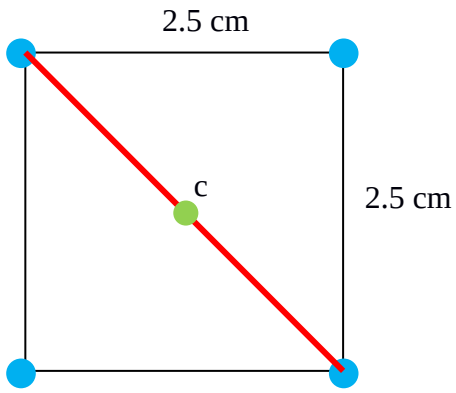

Figure 3.20 Top view of dielectric CCPC

Error Tolerance after installing dielectric CCPC in the mobile solar tracking system,

From the Pythagorean Theorem,

$$c = 3.535534cm$$

Length of center point (Green dot in Figure 3.20) to the blue dot,

$$\frac{c}{2} = 1.7678cm$$

The tolerance of maximum pointing error, γ that we can have in the best case scenario,

$$\gamma = tan^{-1}\frac{1.7678}{45.7}$$
$$\gamma = 2.21525°$$
$$\gamma = 0.03866rad$$
$$\gamma = 38.66mrad \quad (3.7)$$

As illustrated in Figure 3.21, the dielectric CCPC is attached right above the solar cell, the second level concentrated sunlight will never move away from the solar cell. After two levels of concentration, the concentrated sunlight will then transform to the electricity via the solar cell. The amount of current that we collected can be measured by using the multimeter and result will be presented in next chapter.

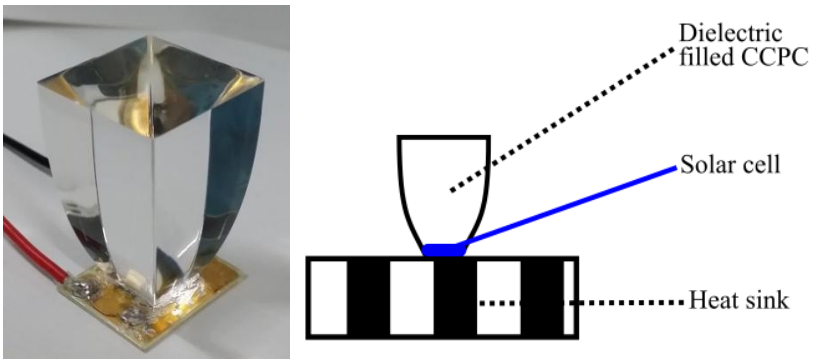

Figure 3.21 Dielectric CCPC and how its install with the solar cell

3.3.1.2 Cooling System

Second level of concentration is attached right above the cooling system. The efficiency of solar cell will be lowered if the temperature of the solar cell is high. Due to this reason, we need a cooling system for the solar cell to maintain the top box portion of the mobile solar tracker at an optimum temperature so that the efficiency of solar cell in electricity generation is not significantly affected. Although we have a heat sink and a fan attached below the solar cell, to maintain the optimum temperature in the top box portion, we designed a circulation cooling system to lower down the temperature inside the top box. We have two fans attached at the bottom part of the top box portion, one fan serves as “fan-in” and the other serves as “fan-out”. This can promote the air circulation at the internal of the top box portion, for the “fan-in” part is to bring in the lower temperature air into the top box and “fan-out” part is to bring the higher temperature air that produced by the concentration activities out of the top box portion. We open two windows at both sides of the top box for us to observe the tracking activities and potential misalignment as well as to perform minor adjustment to the components without taking apart all the parts.

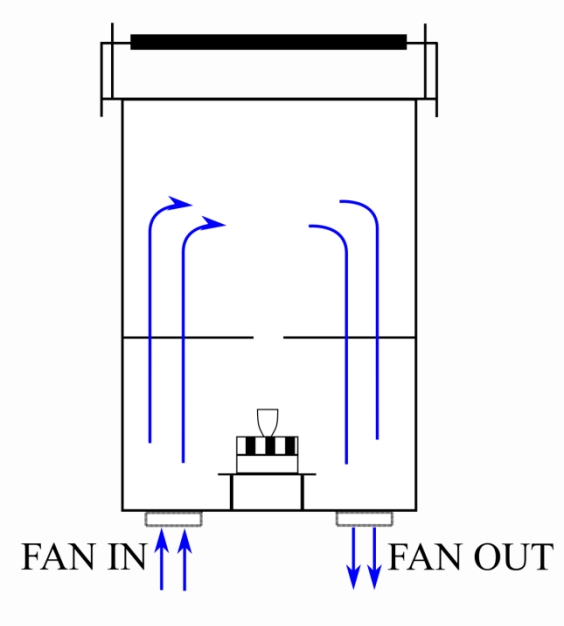

Figure 3.22 Air circulation flow in the top box

Two stepper motors are installed in the mobile solar tracking system. These stepper motors are responded to the Azimuth and Elevation angles respectively. For the Elevation angle, the motor is attached at one side of the top box holder and it will be remaining at 90º upright. As for the Azimuth angle, we have a spinning plate that holding the whole top box portion; this spinning plate has a motor attached right below it. At the initial position, Azimuth will be set at 0º and Elevation will be set at 90º, top view of initialized position of the mobile solar tracker is as Figure 3.24.

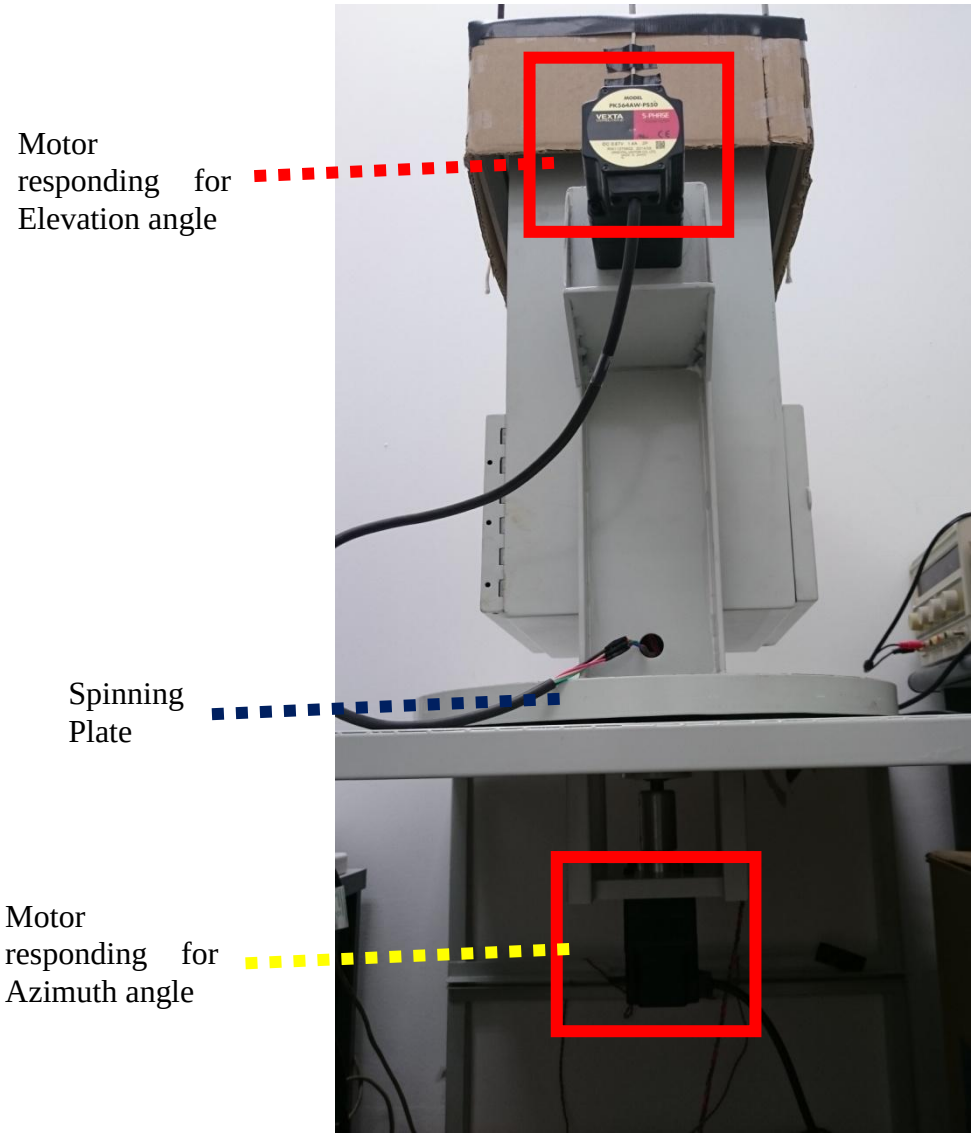

Figure 3.23 Side view of hardware and the motors

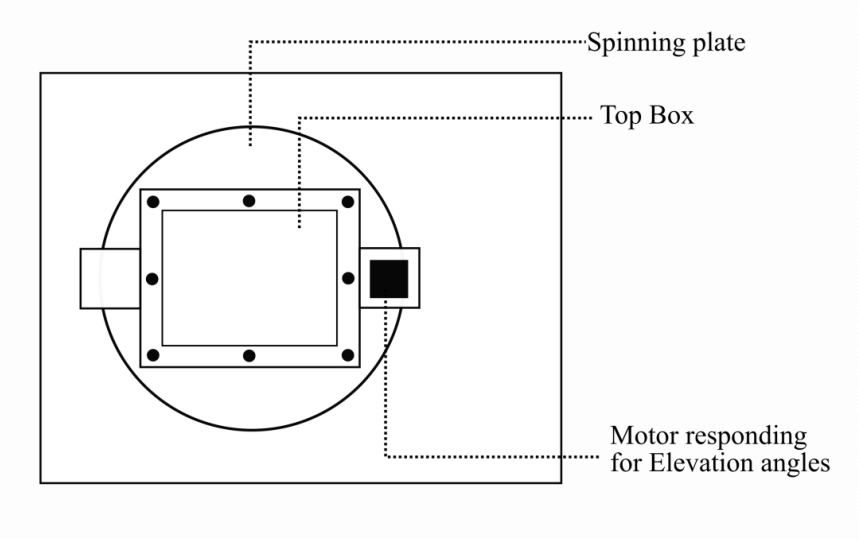

Figure 3.24 Top View of Hardware Initial Position

3.3.2 Controlling Panel

The lowest part of the hardware design is the controlling panel. Controlling panel is where we placed all the components that control the hardware of mobile solar tracker. In our studies, we had Raspberry Pi as the microcontroller that handles all the control in our studies. Raspberry Pi is chosen because it is a stand-alone microcontroller, and it is as small as a credit-card and does not take up lots of spaces in the controlling panel portion. On the other hand, Raspberry Pi has multiple hardware controlling features, users can use the ports easily to control hardware, such as General Purpose Input Output (GPIO), Inter-Integrated Circuit (IIC, I2C), serial ports and so on. In our studies, Raspberry Pi will be controlling the actuation of the solar energy receiver of our mobile solar tracking system based on the timing control modes that we set. Furthermore, as mentioned Raspberry Pi is a microcontroller, it is capable to perform the calculation of the rotational angles

of towards the sun trajectory.

The other important component in the dynamic mobile solar tracking system is digital compass sensor. Digital compass is a magnetic sensor, it measures the magnetic field from the earth and the reading is from 0º to 359º. The readings of 0º, 90º, 180º and 270º corresponds to North, East, South and West respectively. Due to its sensitiveness towards the magnetic field, digital compass sensor cannot be near to any metals or material the affecting the detection of magnetic field, so we ensure that the space of 11” × 11” surrounding the digital compass is left vacant; and the digital compass is placed at the center, aligned with the center point of the top box. It is illustrated in Figure 3.25, the blue line is the center line of the top box and the brown square is the digital compass.

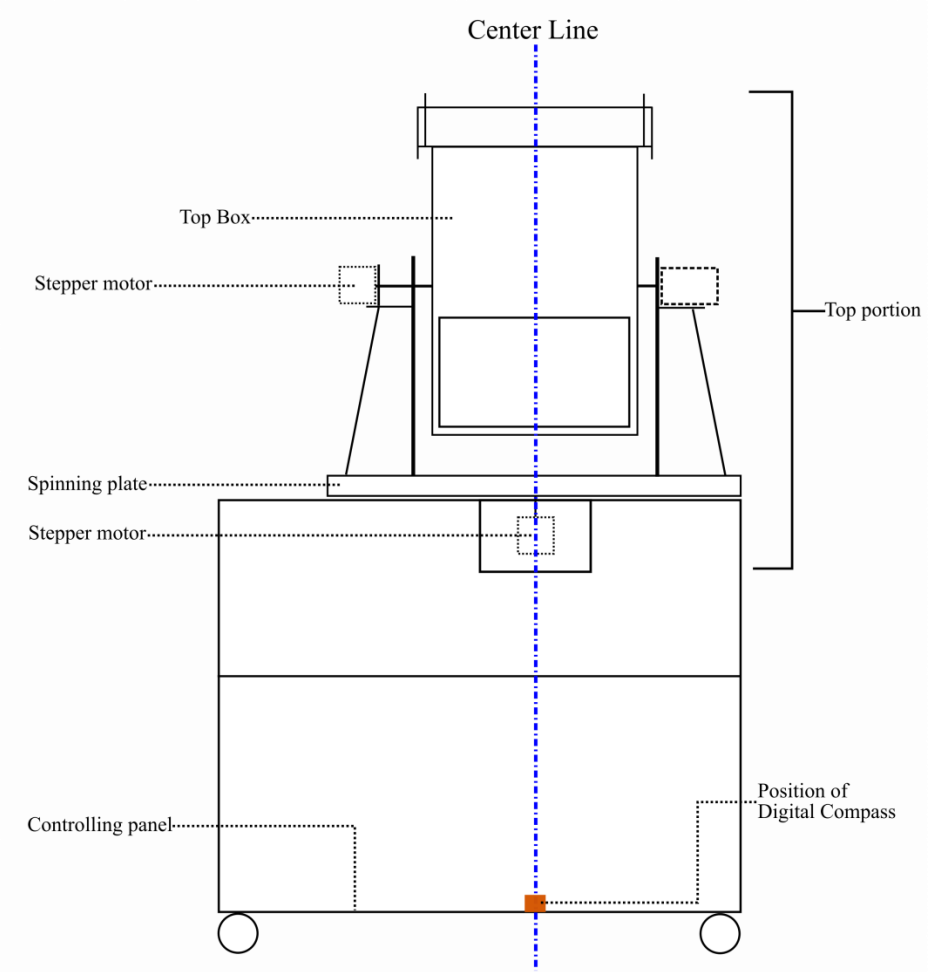

Figure 3.25 Position and alignment of Digital Compass

Another sensor that is important in this study is GPS sensor. The readings of latitude and longitude coordination are important for the calculation of Azimuth and Elevation angles. Both stepper motors need motor driver to provide the pulse control and power to actuate. During the experiment on mobile platform, we had a few portable lithium batteries to provide the power for the motor drivers, so the space is also allocated and Figure 3.26 illustrates the allocation of each component is my design.

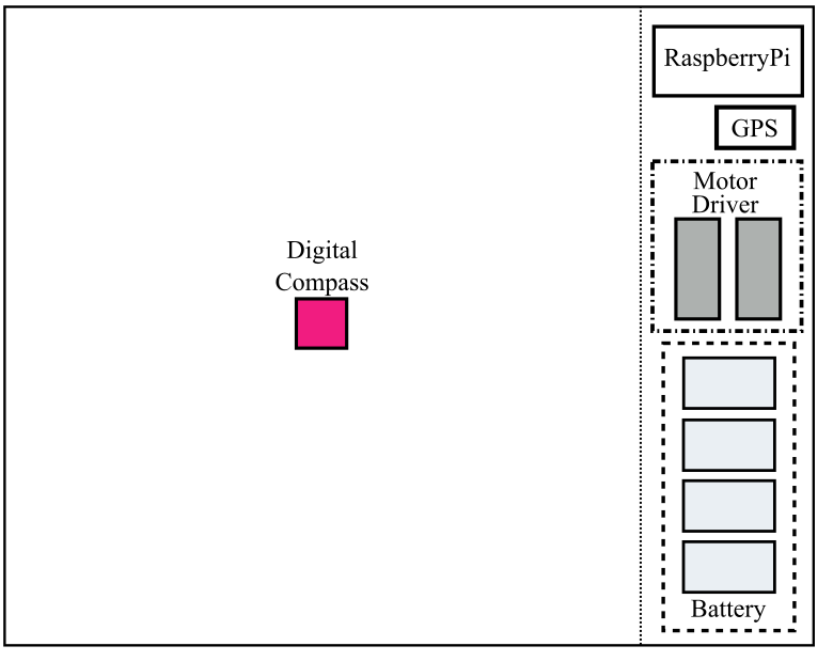

Figure 3.26 Top View of Controlling Panel

3.3.2.1 Raspberry Pi as Controlling System

For both dynamic tracking schemes, Raspberry Pi is used to perform all the control, from collection of sensor readings to the control of the hardware of the mobile solar tracking system. The entire program is written in python language. Every time the Raspberry Pi is booted up, an autorun script will run to initialize the environment variables and load the mobile solar tracking program.

Three physical push buttons and three different color LEDs are included; the first button is to perform the calibration program for digital compass. Digital compass is encouraged to calibrate each time when the system is booted as different positions will have different magnetic fields and

surrounding interference such as metals that can offset the correct readings.

The other two buttons would be the Start and Stop button for the mobile solar tracking program. After the calibration of the digital compass, Raspberry Pi will remain at the idle state and waiting for user to press the Start button to start the mobile solar tracking program. Once the user acknowledges the start of mobile solar tracking program, the system will starts the data acquisition and Red LED and White LED will be turned on. Data acquisition is the collection of the current moving directions by the digital compass. Three sets of readings will be sent to Raspberry Pi for filtering and further calculation. Raspberry Pi will be continuously collecting the readings until it reaches the amounts of readings sufficient for the filtering algorithm to start working. Before the busy looping starts, Raspberry Pi will signal the actuations of motors to park at the initial state of the mobile solar tracking, which is $Azimuth = 0°$ and $Elevation = 90°$. The very first result of the Azimuth and Elevation angles are then set as the reference for the rest of the tracking activity until the Stop button is pressed.

Depending on the timing control of dynamic tracking scheme, the system will check when to update to the latest Azimuth and Elevation angles. If the Time Lapse (TL) mode is chosen, each computed Azimuth and Elevation angles will updated the hardware of the mobile solar tracker and the next loop will only start after current t_L has expired. In the case of Azimuth Actuation Angle (AZ) mode, Raspberry Pi will only trigger the motors to rotate to the latest calculated Azimuth and Elevation angles if the criterion is

met. When the Stop button is pressed, Raspberry Pi will trigger the actuation of both motors to actuate the hardware of the mobile solar tracking system back to the initial position, which $Azimuth = 0°$ and $Elevation = 90°$. After the hardware back to the initial position, the Red LED and White LED will be turned off and the system will remain idle again.

3.4 Automated Image Processing of Solar Images

During the experiments, we captured the sun images as we need to verify the accuracy of our mobile tracking system. The smaller error value of the tracking accuracy means the algorithm that we applied can perform accurate response in tracking the Sun; also it means we can extract the maximum of the sun irradiation. Sun images are captured during the tracking activities; and these images are used in the calculation of the maximum pointing error, also the accuracy of the solar tracking activities based on the real-time captured images. In the measurement of the accuracy of the solar tracking activity, we wrote an automated python image processing program to find the center point of the captured solar images. This method is to make sure there is no biased between the solar images that we captured. Every solar image samples comes with a white patch, which is the “Sun” being we captured, and the blue-coloured background, which is glass paper. The cross placed on the intersection point is acting as the reference towards the center point of the top box portion of our mobile solar tracker hardware.

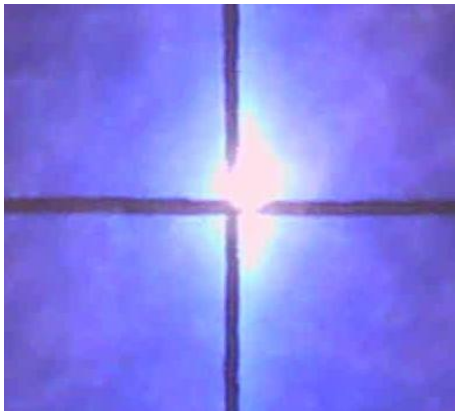

Figure 3.27 Example of sampled solar image

This automated python image processing program, called Self Circle Center Coordinate finder (CCC), mainly processes every solar image that we captured and returns the coordinates of the center of the sun in the images. Before processing the solar image, we find out the main reference which is the pixel coordinates of the intersection point of the cross, in the same image file. Then, the maximum pointing error of all the solar images that we captured can be calculated by finding the distance between the cross and the center of the sun extracted by CCC. For all the solar images that captured, we manually draw a circle that can cover the white patch thoroughly. After drawing the circle on all the solar images, we can run CCC program to process each of the drawn images. The reason behind drawing the circle on each of the solar image is to simplify the detection of the "Sun" on each solar image. Another reference that we need in the calculation of the maximum pointing error of the solar images is the distance between the center point of the highest part top box of the mobile solar tracker hardware and the center position of the CCD camera that we used to capture the solar images.

With the main reference point's pixel coordinates as well as the distance between the center point of top part of top box and center point of CCD camera that we found out from CCC program, it will detect and calculate the center point of the circle that we drew on each solar image. The result of the center point of each solar image is in terms of pixel coordinates. By using the simple arithmetic calculation of distance between two coordinates, we will get the distance in terms of pixel which is subsequently convert to centimeter and milli-radian (mrad) for all the solar images; each pixel equals to 0.02449 centimeters and the result in mrad can be derived from the trigonometry computations described below. Let

$$tan\,\gamma = \frac{\begin{array}{c}converted\ pixel\ difference\ of\\ n\ point\ of\ cross\ to\ the\ \text{Sun}\ captured\end{array}}{\begin{array}{c}distance\ between\ the\ center\ point\ of\ top\ part\ of\ top\ box\\ to\ center\ point\ of\ CCDcamera\end{array}}$$, then we perform $\gamma = tan^{-1}\frac{\begin{array}{c}converted\ pixel\ difference\ of\\ n\ point\ of\ cross\ to\ the\ \text{Sun}\ captured\end{array}}{\begin{array}{c}distance\ between\ the\ center\ point\ of\ top\ part\\ of\ top\ box\ to\ center\ point\ of\ CCDcamera\end{array}}$ getting γ in terms of radian and convert to milli-radian as the result will be in very small decimal place. For example, the pixel distance of one of the solar images is 14.3927 pixels.

Example of Calculation after CCC program,

$$Pixel \rightarrow Centimetre$$

$$14.3927pixels \times 0.02449centimetre = 0.3525centimetre$$

$$tan\gamma = \frac{\begin{array}{c}converted\ pixel\ difference\ of \\ n\ point\ of\ cross\ to\ the\ \text{Sun}\ captured\end{array}}{\begin{array}{c}distance\ between\ the\ center\ point\ of\ top\ part\ of\ top\ box \\ to\ center\ point\ of\ CCDcamera\end{array}} \qquad (3.8)$$

$$tan\gamma = \frac{0.3525cm}{36.5cm}$$

$$\gamma = 9.658mrad$$

The result of maximum pointing error of solar tracking activity will then be saved on an array; from the array we can calculate the average of maximum pointing error in term of hour-based or by daily basis.

CHAPTER FOUR

RESULT AND DISCUSSION

4.0 Result

Based on the design of the mobile solar tracking system, experiments are designed and arranged level by level. Design of mobile solar tracking system is separated to software and hardware. The choice and filtering algorithm are the first priority of the system.

After testing and confirming the hardware and software algorithm of the input of the trajectory calculation, we proceed to the calculation of trajectory angles as well as applying the result into the hardware to test out the algorithm. There is two way to test out the system, one is by measuring the current collected from the solar cell, another is by measuring the accuracy of the solar images capture during the tracking activity.

4.1 Filtering Algorithm

Even though the digital compass remains stationary, the readings still exhibit spikes and noises; hence, filtering algorithms are necessary. However, we encounter difficulty in smoothing discontinuous functions using simple filtering algorithms; e.g. when the reading of the digital compass fluctuates between 0° and 360°, a simple filtering algorithms will produce an incorrect result at around $180°$ which is opposite to the real direction. **Error! Reference**

source not found. shows the reading that we collected from the microcontroller which fed from the digital compass sensor while the digital compass remains stationary.

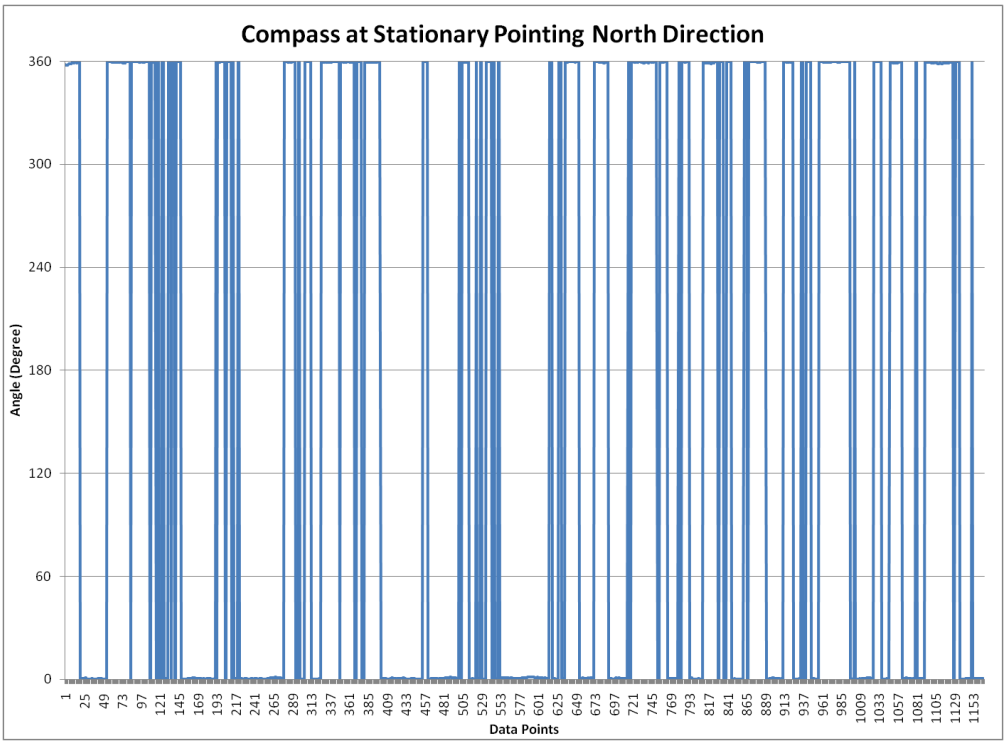

Figure 4.1 Graph of collected readings while digital compass is pointing north direction at stationary

From the figure above, we found out that the fluctuation occurred randomly, without pattern or any significant prediction of change. In terms of readings, we expected a steady reading of 0º when the digital compass is continuously pointing to the north direction. The solution is to convert the raw data readings to a continuous sinusoidal function, as shown in the Figure 4.2, before applying any filtering algorithms. The Y is the raw data reading from the compass.

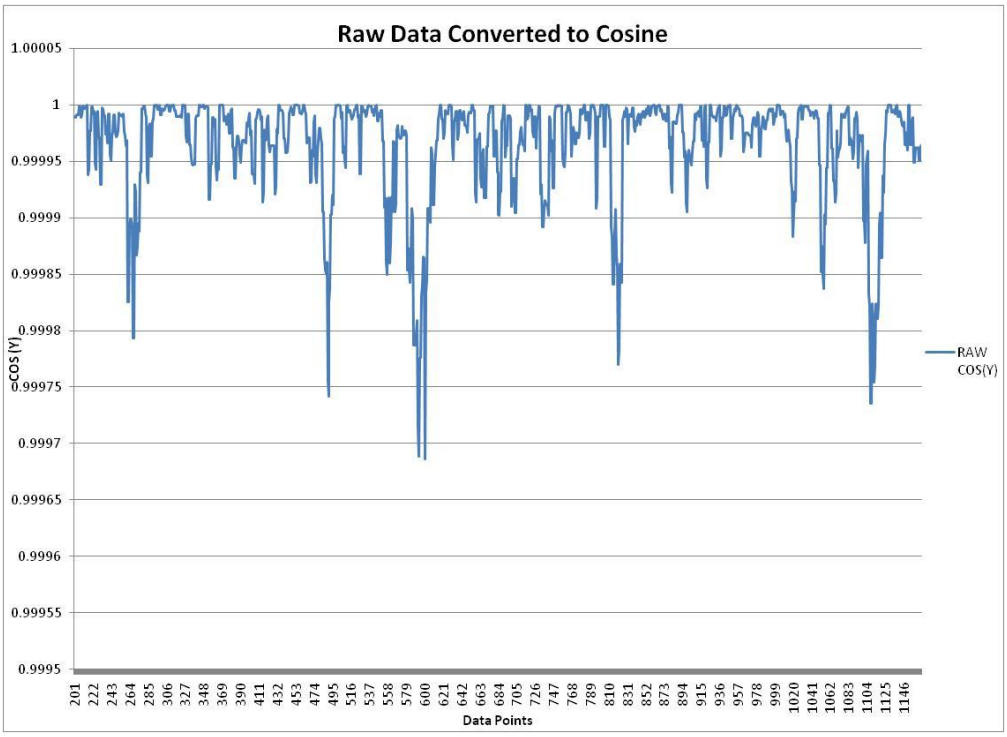

Figure 4.2 Raw digital compass data converted to cosine function

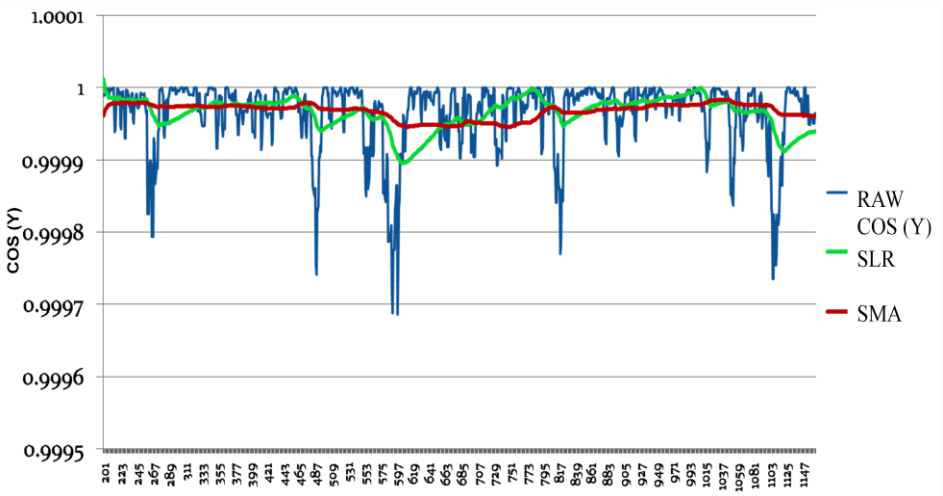

Figure 4.3 Digital Compass reading converted to sinusoidal function (Stationary pointing North)

In Figure 4.3 shows the results of applying two filtering algorithms, Simple Linear Regression (SLR) and Simple Moving Average (SMA), to

cos(Y). It is not obvious which filtering algorithm is a better choice when the compass is in stationary state.

In the next experiment, we collected the digital compass readings while walking according to a rectangular path. This rectangular path can take care the main four directions which are north, east, south and west. We applied SLR and SMA in the result as well and we found out that for filtering using SLR, the prediction is “reacted” too fast and have overshoot during the change of direction or significant change of angle. While for filtering using SMA, the prediction respond is much slower. The filtering algorithm that we developed is come into action. Next, we collected the readings of the digital compass which moves along a rectangular path. The moving direction on each edge of the rectangular path is aligned with north, east, south and west. We applied SLR and SMA to the collected readings and found that the prediction using SLR tends to “overreact” during the change of direction or significant change of angle. While the prediction of SMA responds slower and lags behind the original data. By using the filtering algorithm that we have developed, result is shown in Figure 4.4. Graph below shows the outcome of the filtering algorithm on the raw data collected from the digital compass. This is where the platform moves according to a rectangular path; heading to north from the starting point, moving clockwise and ending heading west returning to the original starting point. This experiment setup is by walking and holding the device facing up on palm. In practice, it is impossible to move perfectly according to a straight line on the road as well as deviation occurs in digital compass while moving of the platform.

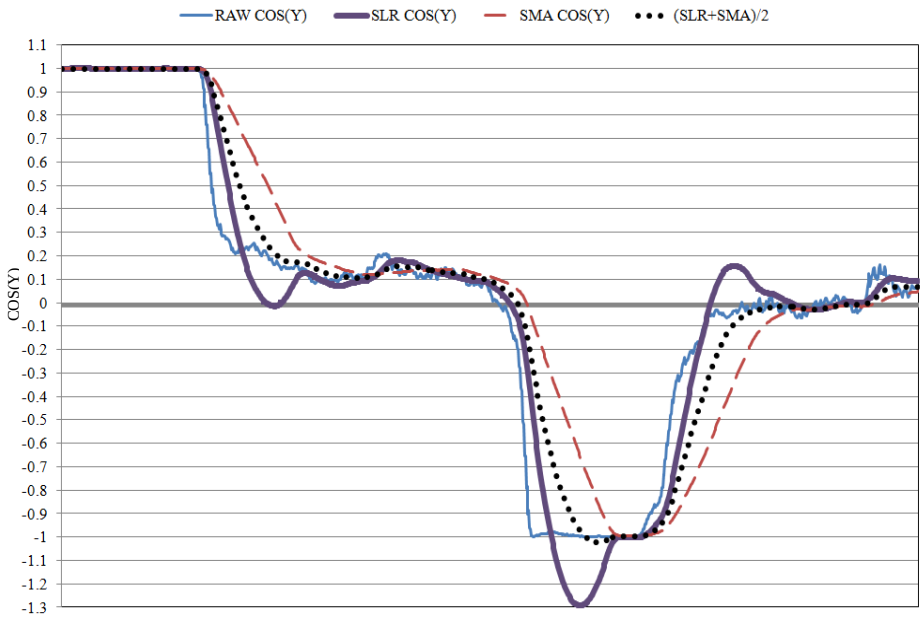

Figure 4.4 Cosined readings Versus Multiple Filtering Algorithms

In spite of that, the readings from the digital compass still very closed the correct values. The Figure 4.4 shows that SLR exhibits overshooting effect before the platform stabilized at the next desired angle (purple line), i.e. from heading north turning to heading east. The overshooting effect is big as the predicted line goes out of the range of sinusoidal function, i.e. [-1, +1]. In the case of SMA (red dashed line), when the change of direction occurs, we can see the prediction line is behind the original cosine data line and gets close to the original cosine data line after the platform has stabilized at the new direction. SMA captures the change of direction much slower as compared to SLR which predicted much faster. The compound filtering algorithm that we developed (black dotted line) embraces the advantages of both algorithms to produce a better filtered result which is smoother and closer to the original cosine data while moving along the straight line as well as upon abrupt change of direction.

Figure 4.5 is another set of digital compass data where we collected it while driving. The main focus of this project is to let the mobile solar tracking system to install and functional on the mobile platforms, so we need to consider and check if the sensor is able to work on the mobile platform and also evaluate the result. We place the Raspberry Pi and OceanServer 3-Axis Digital Compass at one of the back seat of the car, as for the seat beside the driver seat containing metals on the bottom of the cushion. We knew that the digital compass that we are using required being away from metals, so the best position to place the digital compass would be at the back seat. In this experiment, we are trying to run a rectangular path as well, so the map below is one of the locations that really closed to our requirement (Figure 4.6). For this experiment setup, we are driving at around 25 km per hour, on this total distance of 500 meters and we completed the experiment in 5 minutes. Figure 4.5 shows only half of the data we collected as here we are going to show how the abrupt change of direction will affect the original data line as well as the prediction line after the filtering mechanism is applied.

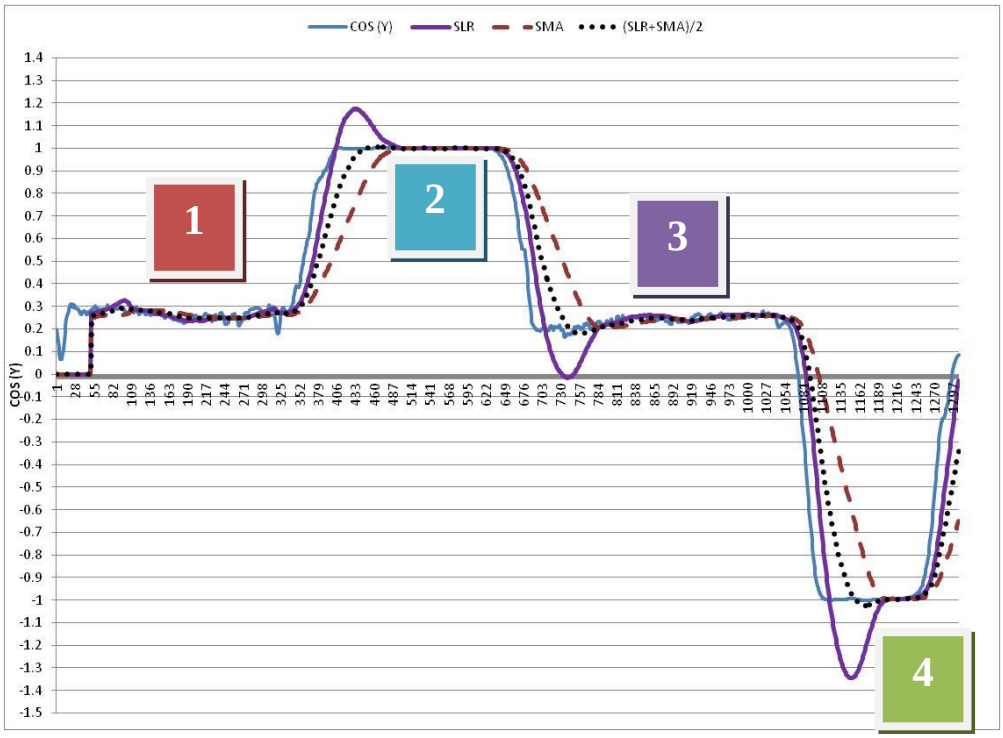

Figure 4.5 Digital Compass data while driving

Figure 4.6 Map of driving path

From this experiment, three filtering algorithms able to smoothen the small fluctuation while the vehicle is moving towards one direction. However, during the abrupt change of direction, we can see that the fluctuation still

occurs even though the digital compass has very high accuracy. For SLR, it breaches the [-1, +1] range of the sinusoidal function while for SMA it responds slow about 80 data points away. The compound filtering algorithm responds faster than SMA and it does not breaches out of the [-1, +1] range, so this prediction line is better compare to SLR and SMA.

4.2 Accuracy of Solar Tracking Activity – Stationary State

To evaluate the effectiveness of the mobile solar tracker, we measure both the maximum pointing error and the short-circuit current along with open-circuit voltage of the solar cell. To calculate the pointing error of the solar tracking activity, a CCD camera is installed on the mobile solar tracker to capture the solar images continuously during the entire period of tracking experiments.

The first experiment is to measure the maximum pointing error of the mobile solar tracker in stationary state. In this experiment, the mobile tracker was set up to point towards South direction instead of North. North direction is one of the alignment that need to be aligned in the non-mobile design, so to show the advantage of our mobile solar tracking system, the Capturing of the solar images is controlled by the Raspberry Pi and out of all the solar images that we took we sampled those which are not shaded by the cloud or any buildings in the surrounding. Figure 4.7 is some of the sampled solar image at different local times.

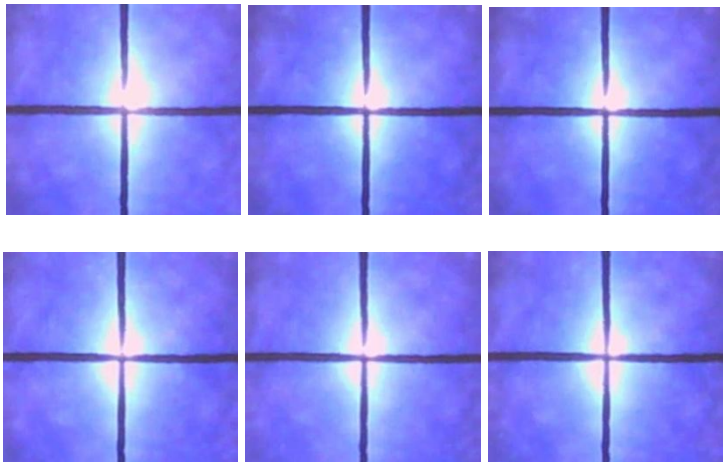

at (a) 12:18:45pm; (b) 12:24:30pm; (c) 12:30:54pm; (d) 12:35:10pm; (e) 12:46:50pm; (f) 12:56:28pm

Figure 4.7 Sampled solar images

This experiment was done on the 13th April 2016 during the peak period when the Sun was nearest to the earth at our current location. The period of the experiment done on 13th April 2016 was short as the sunlight was blocked by a building. Image processing program, CCC program was used to compute the maximum pointing error of solar images of each solar image. Figure 4.8 is the graph of maximum pointing error versus local time.

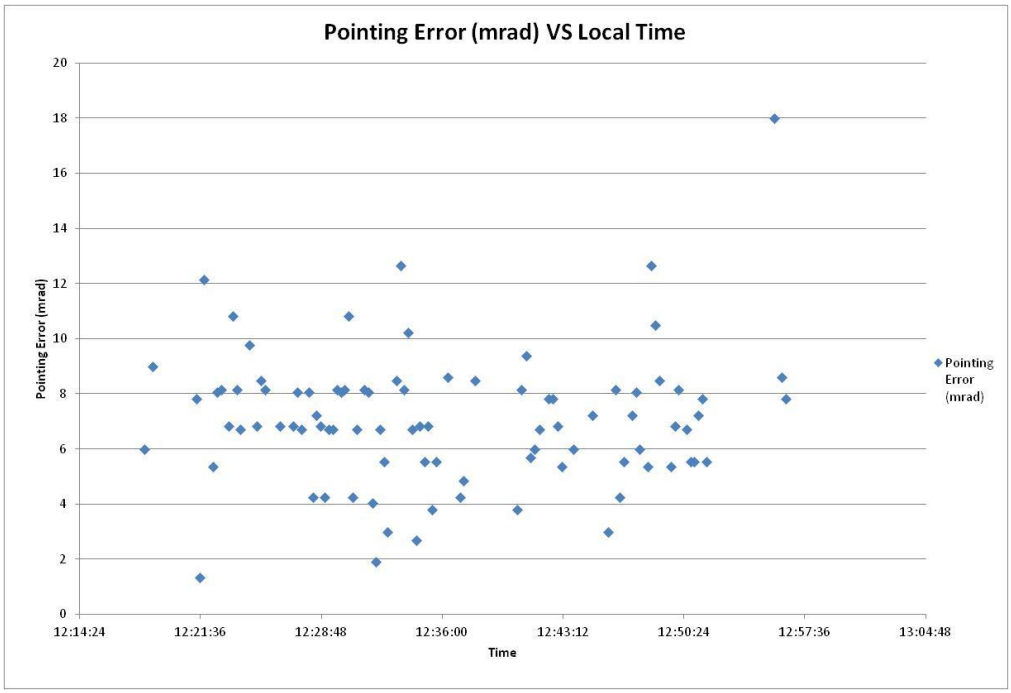

Figure 4.8 Pointing Error versus Local Time on 13th April 2016

The average pointing error of this experiment is 7.117 mrad (Figure 4.8) and we can see most of the time the pointing error is around 4 to 8 mrad, but as the time taken for the experiment was short, we cannot conclude the accuracy of the mobile solar tracking system at stationary state, so we carried out another set of experiment and this experiment took longer time. In this experiment, the time taken is from 10am to 4pm, which covered the peak and non-peak timings. The setup of the mobile solar tracker was the same as the previous experiment. The sampled solar images are as below.

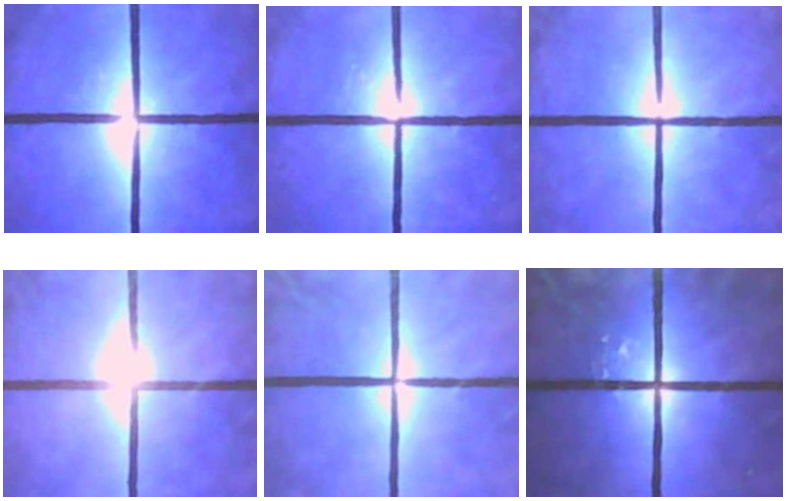

at (a) 10:48:07am; (b) 11:12:55am; (c) 12:14:13pm; (d) 12:32:36pm; (e) 1:57:28pm; (f) 3:37:26pm

Figure 4.9 Sampled solar images

From the sampled solar images, the average pointing error versus local time graph is plotted and the graph in Figure 4.10 shows the average pointing error at each hour. The average maximum pointing error throughout the whole experiment is 8.085 mrad.

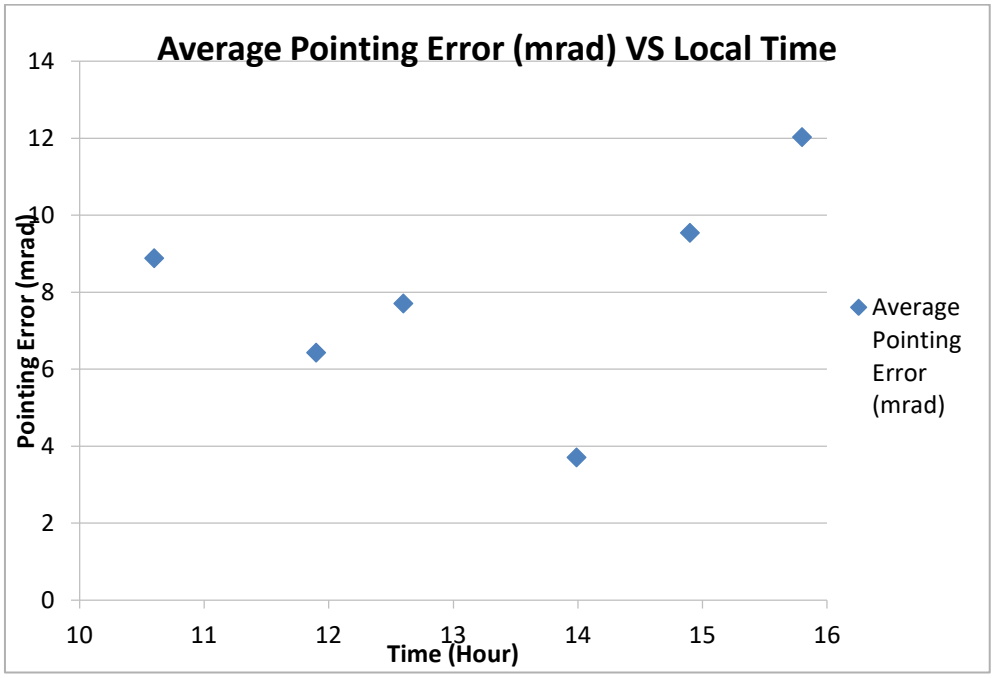

Figure 4.10 Average Maximum Pointing Error versus Local Time by hour

Each point of the graph is the average pointing error at that hour. Total we have six points in the graph above from 10am to 4pm. From the graph, we can know that most of the time the pointing error is mostly below 10mrad and average of pointing error throughout the day is just 0.968mrad (deducting between 8.085mrad and 7.117mrad) more than the previous experiment done during the peak time.

4.3 Accuracy of Solar Tracking Activity – Mobile State

After evaluating the accuracy of the mobile solar tracking system in stationary state, we tested the mobile solar tracking system on a moving platform. In the dynamic solar tracking, we experimented two dynamic timing control modes that we discussed in the methodology. The mobile platform was a truck which has larger enough space for us to monitor the mobile solar tracker onboard. The driving speed of the truck is controlled at around 30 km per hour for all of the experiments. We chose a route as depicted in Figure 4.11 with a total distance of 5km, to increase the probability of getting useable solar images. CCD camera was programmed to capture the solar image right after the motor actuated to the latest calculated Azimuth and Elevation angles; also in between the waiting intervals or after each computation of rotational angles before the actuation decision was made depending on the dynamic timing control mode used during the experiments. First experiment was done by using the time lapse (TL) mode, the timing interval that we used here was 2 minutes; Raspberry Pi ran the program and produced two rotational angles to actuate the motors every two minutes.

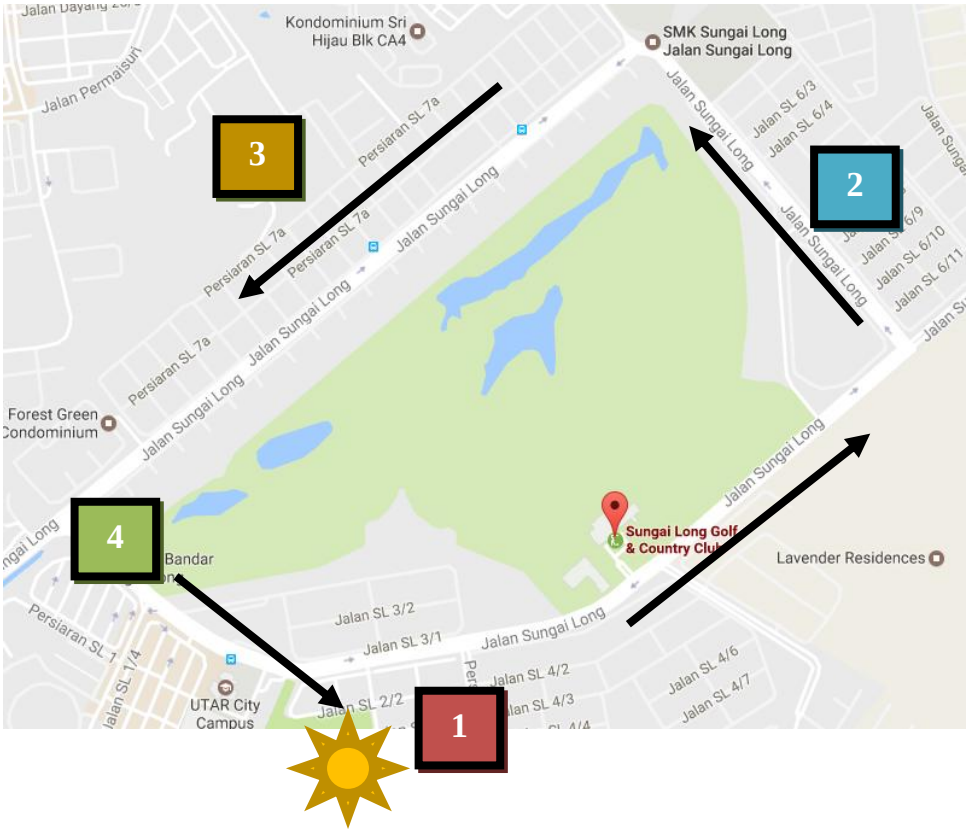

Figure 4.11 Path selected for the experiments on mobile platform

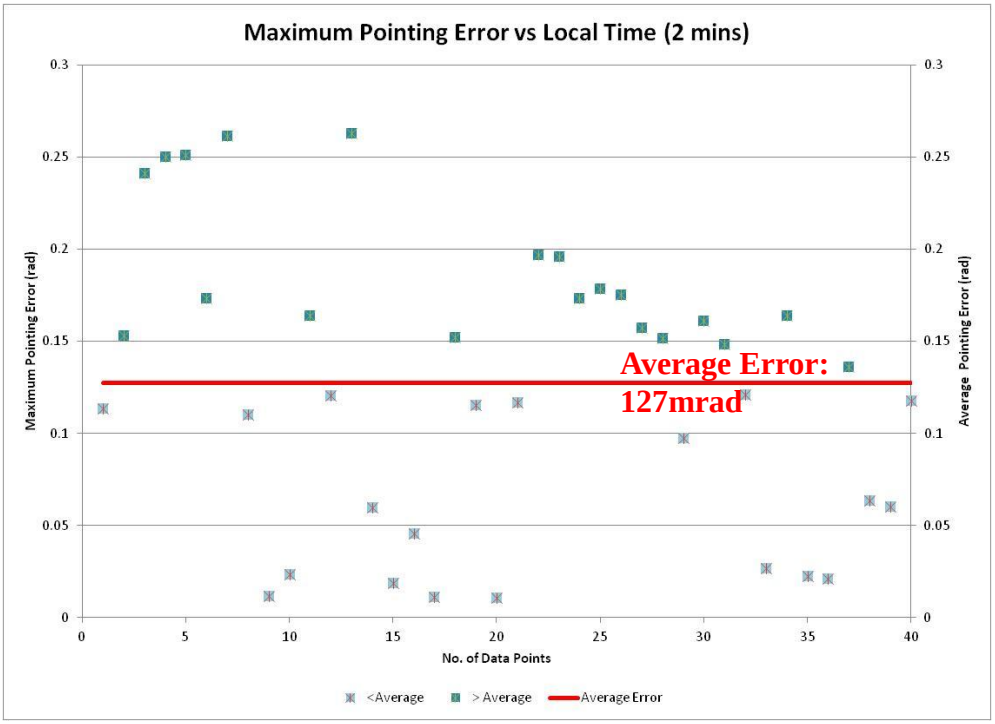

Figure 4.12 Graph of Maximum Pointing Error VS Local Time (TL - 2 minutes)

The red line is the average of the pointing error of the whole experiment. For TL mode, the average pointing error is 127 mrad. The darker markings are those above the red average line while the lighter markings are those below the average line. It is obvious where there are many points that are above the average value, ranging from 100 mrad to 200 mrad, meaning that either the system is lagging or responded too early. In short, the maximum pointing error of the solar tracking activity using TL dynamic timing control mode is above the tolerance value of 38 mrad (referring on the CPV system part in methodology) which we derived previously.

In the next experiments, we experimented the other dynamic control mode which is the Azimuth Actuation Angle (AZ) mode. The experiment setup was the same as the previous experiment; the truck also traveled at around 30 km per hour and followed the same path as shown previously. The threshold value that we applied is 0.1º and 0.5º. Figure is the graph of average pointing error for the AZ mode, with threshold of 0.1º.

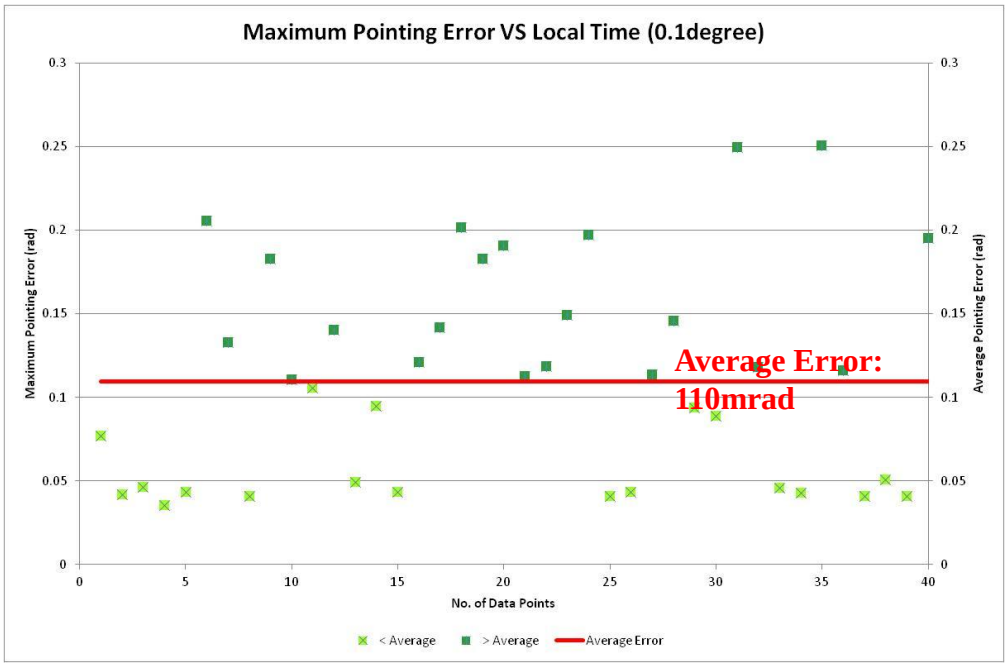

Figure 4.13 Maximum Pointing Error versus Local Time (AZ - 0.1 degree)

In this experiment, the average pointing error dropped significantly to 110 mrad as compared to the previous experiment using TL mode, which is 127 mrad; the red line indicates the average pointing error of this experiment. The number of points scattered above the average line is about half of the points below the line. We cannot make any conclusion from the experiment as for some cases where the mobile solar tracking system was too sensitive and over-responded to slight inclinations or small bumps. As a result, the system needed to make frequent readjustment back to the right directions. This is why the maximum pointing error is not decreasing significantly as compared to the TL mode.

Next, we experimented the AZ dynamic timing control mode using threshold value of 0.5º. The setup of the experiment remained the same as the previous experiment Figure 4.14 Maximum Pointing Error versus Local Time

(AAA - 0.5 degree)is the result of maximum pointing error throughout the whole experiment.

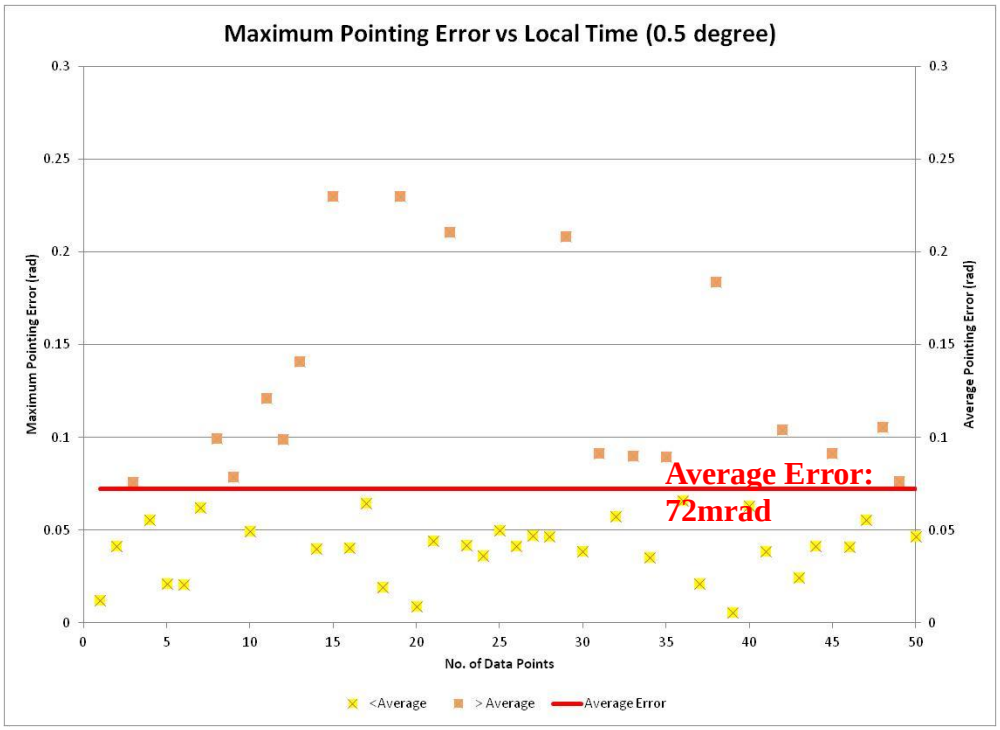

Figure 4.14 Maximum Pointing Error versus Local Time (AAA - 0.5 degree)

From this graph, the average pointing error obviously shifts down to 72 mrad; it is reduced by more than 30% as compared to the AZ mode with 0.1º threshold and more than 40% if compared to the TL mode with waiting period of 2 minutes. The red line is the average maximum pointing error throughout the whole experiment and from the graph, the points scattered above the average pointing error, which is the darker point is much lesser as compared to the previous two experiments. 65% of the points are below the average pointing error line. If the outliers are removed, the average of the pointing error would be much lower as arithmetic averaging can be easily biased by just a few big outliers. AZ mode with 0.5º threshold responded much better

than previous two experiments, because the TL mode cannot constantly update the new Azimuth and Elevation angles, so it obviously lags behind while AZ mode with 0.1º threshold might have cases like over-responding and requires frequent readjustments to adapt to changes in velocity and accelerations plus some environment factors like bumpy road conditions.

If we further analyze the maximum pointing error versus local time at 0.5º, we can know that some of the outlier points are caused by the road conditions, such as small bumps or change of lanes.

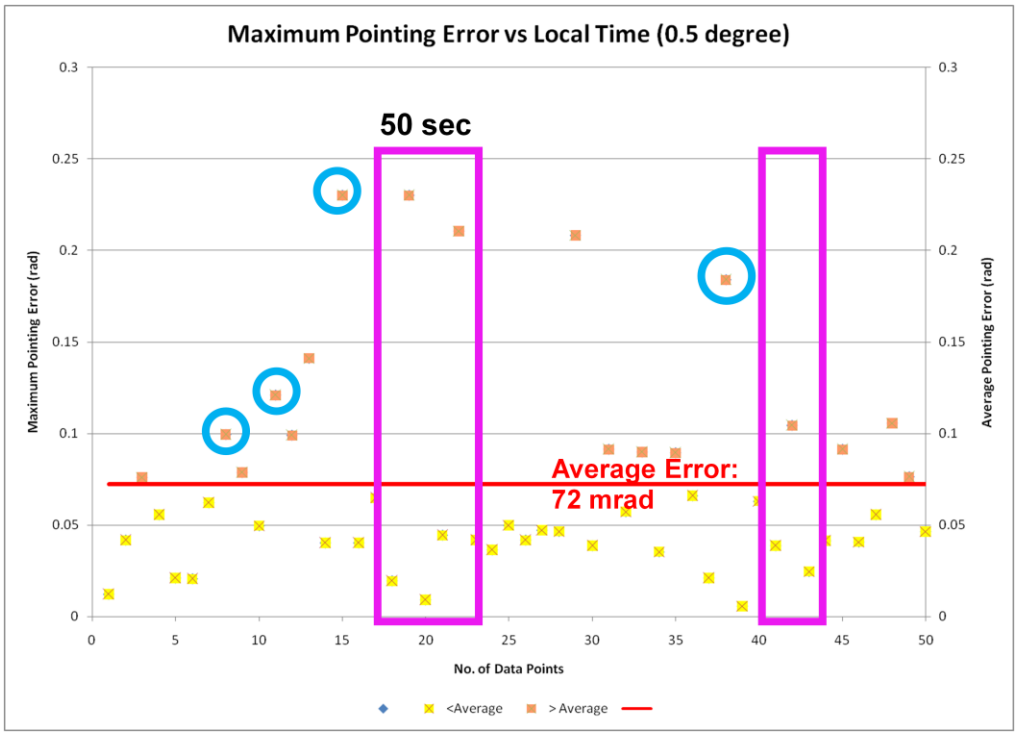

Figure 4.15 Analysis of Road Condition

The two pink squares in Figure 4.15 indicate the change of directions at the turning corners while the blue circles are bumpers on the road on the route we drove. These obvious outliers will pull up the average value even

though majority of the error points are much below the average line as shown in the graph above. If we ignore these significant but rare outliers, we can achieve a higher accuracy. For example, if we drop the outliers above 100 mrad, the average pointing error at becomes 25 mrad. This average pointing error is lower than the maximum tolerance error of 38 mrad. In this case, it means as long the pointing error that we have is lesser than 38 mrad, we can fully absorbing the sunlight without misalignment or wrong direction. The sunlight can be fully concentrated on the dielectric CCPC and from the dielectric CCPC it can perform the second level of concentration effectively.

4.4 Collected Current

Other than getting the accuracy of solar tracking activity, we measured both short-circuit current and open-circuit voltage of the solar cell which was combined with dielectric filled CCPC. These experiments were set up mainly in stationary state. On 1st March 2016, the mobile solar tracker used the TL dynamic timing control mode with the waiting period of 2 minutes (Figure 4.16) while on the 4th March 2016; the system used the same mode with a different waiting period, which is 1 minute (Figure 4.17). The collected current is affected by the weather condition, in both of the experiments, the highest current that we collected is 2.5A, referring to Figure 4.16, after 12:00pm of the day, the value of collected current is gradually getting lesser because the sky is shaded. For the experiment on 4th March 2016, from Figure 4.17, we see that the current value collected is fluctuating because it is a partial cloudy day, although the highest current that we collected is 2.5A; and after 11:58am, there are only some spikes breaching 1.5A but most of the time staying low at 0A.

The average of the open circuit voltage throughout the experiments is 2.8V.

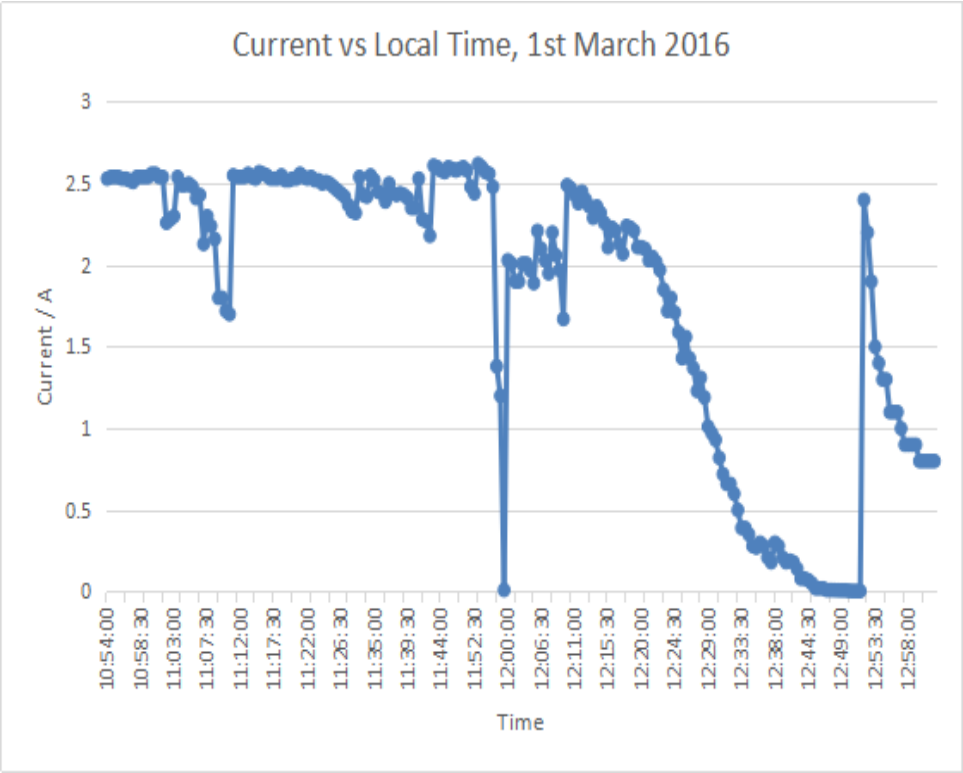

Figure 4.16 Current collected versus Local Time (1st March 2016)

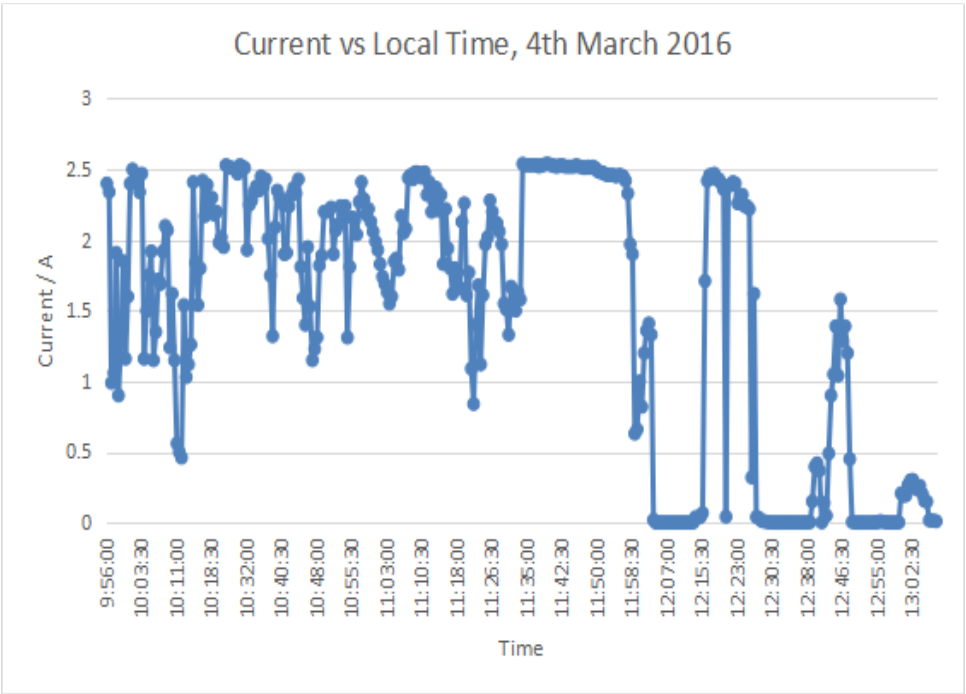

Figure 4.17 Current collected versus Local Time (4th March 2016)

The current collected from the solar cell able to reach 2.5A in both days with seen clear bright sky. However the performance of the solar cell is dropped when the sky is shaded or the weather started to change. Even though Figure 4.16 using TL mode with waiting period of 2 minutes while Figure 4.17 using TL mode with waiting period of 1 minute, solar cell able to collect a current value of 2.5A with bright moment although it is a cloudy day. The open circuit voltage is remains at 2.8V meaning the cooling system is stable throughout the collection of sun irradiation and maintains the performance of solar cell.

CHAPTER FIVE

CONCLUSION AND FUTURE WORK

5.0 Conclusion and Future Work

5.1 Conclusion

The three research objectives are achieved. First, completion of software and hardware design prototype to test proves of the idea of mobile solar tracking system on mobile platforms. In this project, we proposed a new sun tracking algorithm for mobile solar tracking system. We found that a mobile solar tracking system can be built on top of the General Formula of Sun Tracking by adding two hardwares, i.e. GPS sensor and the digital compass, to keep track of geographical and moving direction changes of the mobile platform. During the implementation of the sensors, we found that a mechanism to filter the noises in the sensors is important to the accuracy of mobile tracking; we have developed a compound filtering algorithm to remove noises in the readings from digital compass before passing the values to the general formula of sun tracking.

For the solar energy receiver, CPV system that used in the study is a two-level concentration system, first level use the Fresnel lens and the second level use the dielectric filled CCPC. It is to increase the probability of getting the sun irradiance as the second level of concentration, the dielectric filled CCPC, give us a better pointing error tolerance of 38 mrad. This tolerance is

important for the mobile solar tracking system to work effectively as mobile platform does not constantly move on one single direction.

In the design of the hardware and software of the system, we have considered and evaluated the ability and performance of each of the components and we use Raspberry Pi as main microcontroller to control the whole system. Raspberry Pi is able to work alone and does the computation of the rotational angles as well as the dynamic control of the motors' actuation. The dynamic timing control of the motors' actuation we had included two modes in the study and the performance is measured based on the solar images that we captured during the solar tracking activity. The second and the third objectives are achieved. The tracking performance of the mobile solar tracking system is analyze by capturing the sun image and calculating the pointing error, also collecting the current and voltage reading from solar cell. For the evaluation, our result found that AZ with 0.5º achieve the lowest average pointing error which is 72mrad as compared to the other two experiments which are AZ with 0.1º and TL by 2 minutes.

5.2 Future Work

In this study, the mobile solar tracking system is designed without any feedback system, as it is based on the digital compass reading and GPS readings to calculate the rotational angles. Current experiments are limited to small driving area; it is possible that the result might vary if the mobile solar tracking system is tested on a longer traveling distance and time. Therefore, if feasible it would be better to include an encoder feedback control in the

implementation to make sure the mobile solar tracking system to reduce the tracking errors and maximize the solar energy received.

The hardware design of the mobile solar tracking system in this study is the first prototype, for future design, the size of the hardware of mobile solar tracking system can be reduced or enlarged based on the user choice. On the other hand, the choice of material of the hardware can be reconsidered to make sure this mobile solar tracking system can fulfill the study objective whereby everyone can own this personal mobile power generation system.

For future work, the components and microcontroller of the mobile solar tracking system can be implemented on a mounted controller. This is the customization after all the components are can be confirmed. External user controls such as calibration, time and date collection or some of the internal data collection, start and stop control of the mobile solar tracking system can be done by using physical push buttons or switches; also some LED or simple indication to show the users the mobile solar tracker is running at which process or state at the moment. This indication can simplify the use of mobile solar tracking system and keep it user-friendly.

The size and material can be reconsidered; also the solar energy receiver can be replaced by any other type of solar energy receiver than the single two-level CPV system implemented in this system. From the experiment in this study, the focus of the performance analysis of the mobile solar tracking system is based on the tracking accuracy. If the error of the

tracking accuracy is small, meaning that under a good condition, weather with high sun radiation, the solar energy receiver can receive maximum sun radiation, no matter which type of solar energy receiver is used. Some of the possible solar energy receiver can be implemented such as single level CPV system, single solar panel, arrays of solar cells or array of solar panels. The choice of the solar energy receiver is depending on the purpose of the mobile solar tracking system. For example, solar panel can replace our two levels CPV system to fit into the design of the mobile home system which is popular in US.

Currently, the system uses only one of the dynamic tracking modes at one time. For future work, two dynamic tracking modes can be combined. For some period, it is no need for the system to keep calculating the new rotational angles. For instance, Time Lapse (TL) mode can be used before solar time reaching 11:00am and after 1:00pm whereas Azimuth Actuation Angle (AZ) mode can be used in between 11:00am and 1:00pm as AZ mode keep tracks of the sun trajectory much faster than TL mode.

Furthermore, our method can improve the effectiveness of offshore solar tracking systems which are often affected by unexpected drifts in orientations.

References

Abdallah, S. & Nijmeh, S., 2004. Two axes sun tracking system with PLC control. *Energy Conversion Manage,* Volume 45, pp. 1931-1939.

Adib, R. et al., 2016. *Renewables 2016 Global Status Report,* Paris: Frankfurt School UNEP Collaborating Centre for Climate & Sustainable Energy Finance.

Aiuchi, K. et al., 2006. Sensor-controlled heliostat with an equatorial mount. *Solar Energy,* Volume 80, pp. 1089-1097.

Akhmedyarov, K. et al., 1986. G.,Economic efficiency of the FV-500 solar photoelectric station with automatic tracking of the sun. *Solar Energy,* Volume 22, pp. 44-47.

Association, S. E. I., n.d. *Concentrating Solar Power.* [Online]
Available at: http://www.seia.org/policy/solar-technology/concentrating-solar-power
[Accessed 2016].

BrightSource Limitless, 2014. *Ivanpah Project Fact,* California: BrightSource Limitless.

Brilliant Harvest, 2016. *Brilliant Harvest.* [Online]
Available at: http://www.brilliantharvest.com/2016/04/qa-skinny-solar-panels/
[Accessed 11 2016].

Bushong, S., 2016. *Advantages and Disadvantages of Solar Tracker System.* [Online]
Available at: https://www.solarpowerworldonline.com/2016/05/advantages-disadvantages-solar-tracker-system/
[Accessed 2016].

Chen, F., Feng, J. & Hong, Z., 2006. Digital sun sensor based on the optical vernier measuring principle. *Meas. Sci. Technol.,* Volume 17, pp. 2494-2498.

Cheng, T. C., Yang, C. K. & Lin, I., 2016. Biaxial-Type Concentrated Solar Tracking System with a Fresnel Lens for Solar-Thermal Applications. *Applied Sciences,* 6(115).

Chong, K. & Wong, C., 2009. General Formula for on-axis sun-tracking system and its application in improving tracking accuracy of solar collector. *Solar Energy,* Volume 83, pp. 298-305.

Fedkin, M., 2016. *Why tracking?*. [Online]
Available at: https://www.e-education.psu.edu/eme812/node/519
[Accessed 2016].

Ferdaus, R. A., Mohammed, M.A, Rahman, S, Salehin, S., AbdulMannan, M., 2014. Energy Efficient Hybrid Dual Axis Solar Tracking System. *Journal of Renewable Energy,* Volume 2014.

Golubova, A., 2016. *Large-Scale Solar Heating & Energy Storage System Installed at Mexican Peñoles' Mine.* [Online]
Available at: http://energyandmines.com/2016/10/large-scale-solar-heating-energy-storage-system-installed-at-mexican-penoles-mine/
[Accessed 2016].

Huang, H., Su, Y., Gao, Y. & Riffat, S., 2011. Design analysis of a Fresnel lens concentrating PV cell. *International Journal of Low-Carbon Technologies,* 6(3), p. 165–170.

Ingole, A. N., 2016. Arduino Based Solar Tracking System. *Satellite Conference ICSTSD 2016 International Conference on Science and Technology for Sustainable Development,* pp. 61-66.

Kok-Keong Chong, Chee-Woon Wong, Fei-Lu Siaw, Tiong-Keat Yew, See-Seng Ng, Meng-Suan Liang, Yun-Seng Lim and Sing-Liong Lau, 2009. Integration of an On-Axis General Sun-Tracking Formula in the. *Sensors,* Volume 9, pp. 7849-7865.

Kribus, A., Vishnevetsky, I., Yogev, A. & Rubinov, T., 2004. Closed loop control of heliostats. *Energy,* Volume 29, pp. 905-913.

Lai, A.C., Chong, K.K., Ho, M.C., Yap, S.H., Heng, C.K., Lim, B.H., Lee, J.V. 2014. A Generic Sun-Tracking Algorithm for On-Axis Solar Collector in Mobile Platforms. *The National Physics Conference.*

Leone, S., 2011. *Can HCPV Compete with Low-Cost PV Panels?.* [Online] Available at: http://www.renewableenergyworld.com/articles/print/volume-15/issue-5/solar-energy/can-hcpv-compete-with-low-cost-pv-panels.html [Accessed 2016].

Lewis, C., 2016. *Top 5 solar farms in the world | Top 10 | Energy Digital.* [Online]
Available at: http://www.energydigital.com/top-10/top-5-solar-farms-world [Accessed 2016].

Luque-Heredia, I., Cervantes, R. & Quéméré, G., 2006. *A sun tracking error monitor for photovoltaic concentrators.* Waikoloa Village, s.n.

Luque-Heredia, I., Gordillo, F. & Rodriguez, F., 2004. *A PI based hybrid sun tracking algorithm for photovoltaic concentration.* Paris, s.n.

M.E., S.Sivasakthi; E.Vinodha, T.Vasanthakumari, D.Vinitha, P.Balakavi, 2016. *Automatic solar tracking system for power generation using microcontroller and sensor.*. s.l., s.n.

Mercer, M. B., 2012. *Concentrated Solar Power:Parabolic Dish.* [Online] Available at: https://www.mtholyoke.edu/~wang30y/csp/ParabolicDish.html [Accessed 2016].

Nuwayhid, R., Mrad, F. & Abu-Said, R., 2001. The realization of a simple solar tracking concentrator for the university research applications. *Renewable Energy,* Volume 24, pp. 207-222.

Ogden Publishing Corporation, 2015. *WSU Engineers Create Solar Generator, Charging Station.* [Online]
Available at: http://www.weber.edu/east/engineers_create.html

[Accessed 2016].

P.Rodrigoa, E.F.Fernández, F.Almonacid & P.J.Pérez-Higueras, 2013. Models for the electrical characterization of high concentration photovoltaic cells and modules: A review. *Renewable and Sustainable Energy Reviews,* Volume 26, pp. 752-760.

Parkinson, G., 2013. *How it works: Solar power towers with integrated storage.* [Online]
Available at: http://reneweconomy.com.au/how-it-works-solar-power-towers-with-integrated-storage-78892/
[Accessed 2016].

Roman, R. J., Peterson, J. E. & Goswami, D. Y., 1995. An Off-Axis Cassegrain Optimal Design for Short Focal Length Parabolic Solar Concentrators. *Journal of Solar Energy Engineering,* 117(1), pp. 51-56.

Roselund, C., 2013. *Solar Energy System of the Month - Large-scale PV comes to Ukraine.* [Online]
Available at: http://www.solarserver.com/solar-magazine/solar-energy-system-of-the-month/large-scale-pv-comes-to-the-ukraine-activ-solars-ohotnikovo-and-perovo-pv-plants.html
[Accessed 2016].

Rubio, F., Ortega, M., Gordillo, F. & Lopez-Martinez, M., 2007. Application of New Control Strategies for Sun Tracking. *Energy Conver. Manage,* Volume 48, pp. 2174-2184.

Samuel, B., B.Bharathi & J.Mrudula, 2013. Design of PC Controlled Automatic Solar Tracker Robot. *International Journal of Innovative Research in Science, Engineering and Technology,* 2(10), pp. 5300-5304.

Sanchez Vega, L. R., 2016. Modeling and experimental evaluation of a small-scale fresnel solar concentrator system. *Renewables: Wind, Water, and Solar.*

Schultz, R., Dyk, E. v. & Vorster, F., 2012. *The Design of a High Concentrator Photovoltaic Module (HCPV) ,* s.l.: s.n.

Shanks, K., Sarmah, N., Reddy, K. S. & Mallick, T., 2015. The Design Of A Parabolic Reflector System With High Tracking Tolerance For High Solar Concentration. *American Institute of Physics,* 1616(1), pp. 211-214.

SkyFuel, Inc., n.d. *Our Technology - Why Parabolic Trough?.* [Online]
Available at: http://www.skyfuel.com/why-parabolic-trough.shtml
[Accessed 2016].

SolarInsure, n.d. *Top 5 Largest Solar Power Plants of the World.* [Online]
Available at: http://www.solarinsure.com/largest-solar-power-plants
[Accessed 2016].

Thomas, C., 2009. Fuel Cell and Battery Electric Vehicle Compared. *International Journal of Hydrogen Energy,* Volume 15, pp. 6005-6020.

Thompson, A., 2016. *The World's Largest Solar Plant Is Now Online in India.* [Online]
Available at: http://www.popularmechanics.com/science/green-tech/a24063/worlds-largest-solar-plant-india/
[Accessed 2016].

U.S. Department of Energy, 2011. *MOJAVE.* [Online]
Available at: https://energy.gov/lpo/mojave
[Accessed 2016].

U.S. Department of Energy, 2013. *Dish/Engine System Concentrating Solar Power Basics.* [Online]
Available at: https://energy.gov/eere/energybasics/articles/dishengine-system-concentrating-solar-power-basics
[Accessed 2016].

U.S. Department of Energy, 2013. *Energy Efficiency & Renewable Energy of the U.S DOE and Office of Transportation & Air Quality of U.S. EPA,* s.l.: The Official U.S. Government Source for Fuel Economy Information.

V.D.Rumyantsev, et al., 2010. *HCPV Modules With Primary And Secondary Minilens Panels,* s.l.: s.n.

Wang, Y., 2008. *Concentrated Solar Power - Parabolic Trough Poewr Plant.* [Online]
Available at: https://www.mtholyoke.edu/~wang30y/csp/PTPP.html
[Accessed 2016].

Zhang, Y., Yang, H, Jiang, P., Mao, S., Yu, M., 2016. Research on a square Cassegrain-type solar concentrating reflector with a double pyramid. *Optica Applicata,* XLVI(3), pp. 461-471.

Zipp, K., 2013. *What is a solar tracker?.* [Online]
Available at: https://www.solarpowerworldonline.com/2013/04/how-does-a-solar-tracker-work/
[Accessed 2016].

APPENDIX A

Specification of OceanServer US5000USD 3 Axis Digital Compass

Parameter	Value
Azimuth Accuracy	< 0.5ºRMS Heading while level, undisturbed field, 0.1º resolution
Inclination Accuracy	Typical 1º accuracy <±30º tilt
Inclination range	±80º (Output for full rotation at decreased accuracy pitch ±90º, roll ±180º)
Temperature range	Accuracy specified for 0°C to 50°C, -40°C to +85°C operation (decreased accuracy at temp extremes) Humidity: 20-80% RH non-condensing
Shock (Operating)	3,000 G, 0.5 ms, 10,000 G 0.1 ms
Data Refresh Rate	0.01 Hz to 40Hz sentence output rate
Size	1” x 1” x 0.3” module

Weight	~ 2 grams
Supply Voltage	3.3V – 5VDC (Will operate with up to 15VDC using 3× the power)
Power consumption	35 ma @5V (-US variant, in USB mode)
Serial Data Interface	RS-232C levels, TTL and USB 2.0 based on Variant 4800 – 115000 baud, 8 bit, 1 stop, no parity (19200 default)
Sentence Format	NMEA0183 Style, four sentence formats, supporting xor parity ($HCHDT, $OHPR, $C, comma delimited. Supports Acceleration & Magnetic sensor output in X,Y,Z
Magnetic Compensation	Hard Iron and Soft Iron calibrations
Routines	Supported, note: Soft iron (V1.4 or later firmware)